Development of Hexaaluminate Catalysis for High Temperature Catalytic Combustion
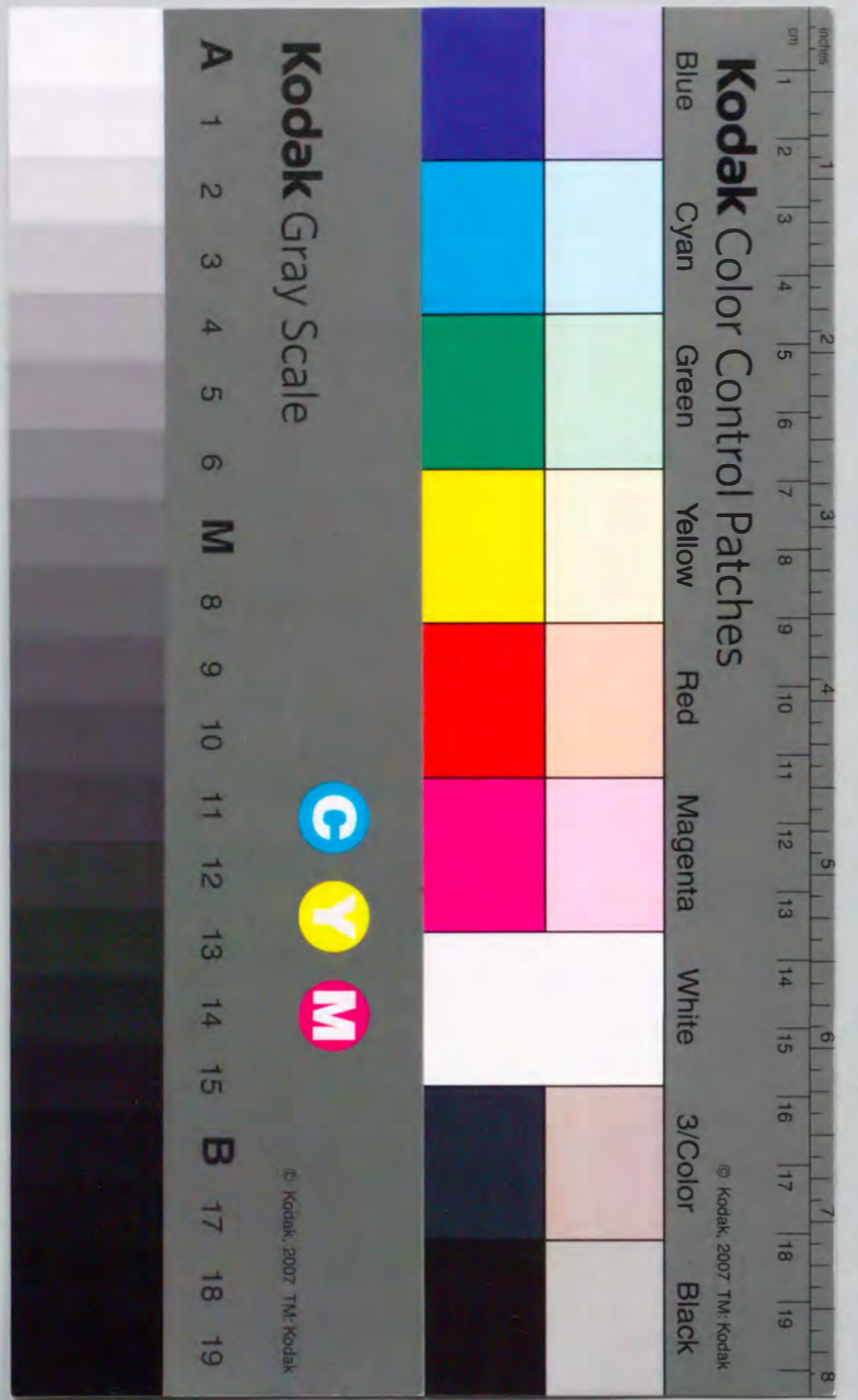
町田, 正人

Development of Hexaaluminate Catalysts for High Temperature Catalytic Combustion

Masato Machida

Development of Hexaaluminate Catalysts for

High Temperature Catalytic Combustion

Masato Machida

Kyushu University

1991

Table of Contents

Chapter 1

INTRODUCTORY SURVEY

1.1 General Background

Today, much of the world's energy need for the power genera-
tion depends on the combustion of fossil fuels. On the other
hand, combustion systems have caused various problems of environ-
mental disruption. One of the most serious emission gases is
nitrogen oxide (NO_X), which causes an acid rain. The forest
damage due to the acid rain has become a hot issue in the world.
Carbon dioxide leading to the greenhouse effect is another big
target of environmental protection. We can not expect the dra-
matic reduction of carbon dioxide as long as we use fossil fuels.
In this circumstance, increasing energy efficiency is quite
important to reduce the emission of carbon dioxide.

To settle these global environment and energy issues, the
combustion systems need to be much improved for a high efficiency
and low emissions.[1-3] Catalytic combustion has been proposed and
developed as the method of promoting fuel-lean combustion with a
minimum pollutant formation. The term, catalytic combustion,
generally means the complete oxidation of fuels over solid cata-
lysts regardless of chemical reaction mechanisms. But, purely
catalytic processes can not achieve the high performance require-
ments demanded by commercial combustors, such as a gas turbine.
A possible process for attaining these objectives is "catalyti-
cally stabilized thermal combustion", which demonstrates the
exceptional performance due to the combination of features of
both catalytic oxidation and gas-phase combustion. [4,5]

The use of oxidation catalysts in a combustor has been an important subject for researchers of catalysis and combustion since the 1970's, particularly in the United States. To date there have been five international workshops, many technical papers and review articles[6-14] devoted to catalytically stabilized thermal combustion. While preliminary results have been quite promising,[15-17] there are several problems still remaining to be solved prior to practical applications. First, catalyst materials with the sufficient heat resistance have not been developed. Since the catalytic combustion is operated above 1200 ℃, conventional catalysts, such as supported noble metals, can be hardly used because of the thermal deactivation. Secondly, the catalytic combustion mechanism is not well understood because of the complex interaction between heat and mass transfer processes and elemental reactions. The elucidation of combustion mechanism is strongly necessary for the optimal combustor design. However, the second problem also depends on the development of catalyst materials which can be used for the reaction at high temperatures. The catalyst with high thermal stability is indispensable for the whole study of high-temperature catalytic combustion.

1.1.1 Principle of Catalytic Combustion

A catalytic combustor consists of a catalyst bed through which a premixed and preheated fuel/air mixture is passed (Fig. 1.1).[18-20] Figure 1.2 shows the corresponding reaction rate of catalytic combustion. In the front part of the catalyst bed, where the catalyst temperature is low, combustion starts as a surface reaction (region a). After initiation of surface reactions, the reaction rate is going to be high with an increase in
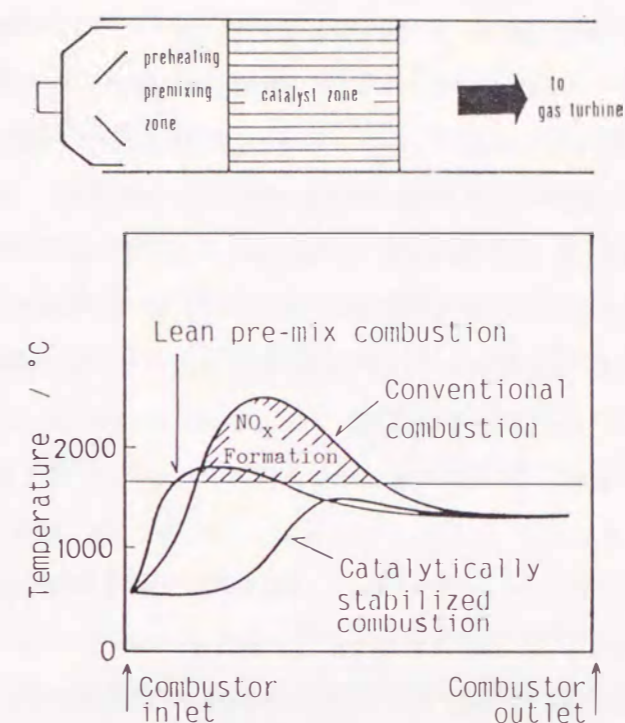

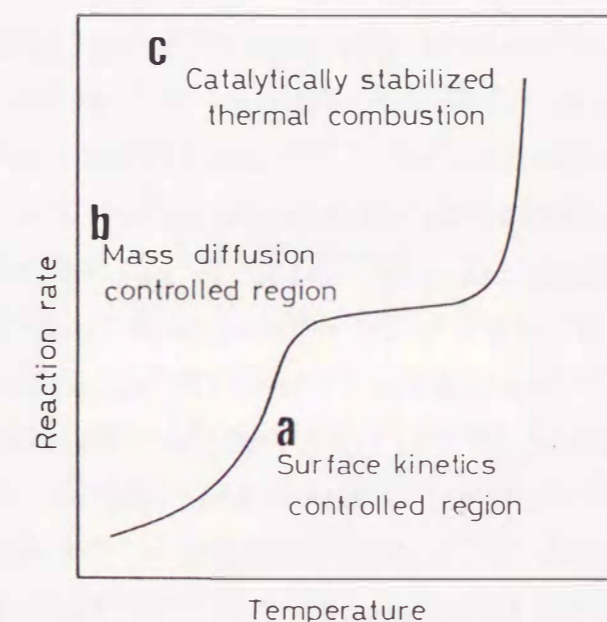Fig. 1.1. Schematic profiles of temperature and NO_x emission in a combustor.

Fig. 1.2. Temperature dependence of overall reaction rate in catalytic combustion.

temperature so that the overall process is limited by the rate of mass transport to the surface (region b). In this region, the observed reaction rate levels off with increasing the temperature because the mass transfer coefficient is a rather weak function of temperature. For more active catalysts or for richer fuel concentrations, the mass transfer limitation could be observed more easily. As the exothermic surface reaction proceeds further, the axial catalyst temperature increases and consequently, the radical reaction will be initiated at some points in the catalyst bed. Then, bulk gas temperature becomes so high that the gas-phase reactions occur simultaneously with the catalytic reactions and the combustion goes to completion (region c).

The resultant axial temperature gradients in the catalytic combustor are compared to that in the conventional flame combustor in Fig. 1.1. The catalytic combustion can reduce the peak of combustion temperature unless lowering the combustor performance because the high heat release rate can be attained by the catalytically-stabilized homogeneous gas-phase combustion. Thus, in the high temperature catalytic combustion, gas-phase combustion dominates the overall reaction rate. This is the most different feature from other conventional catalytic processes. Although the high temperature catalytic combustion is one of the gas-phase combustion, the catalyst plays a very important role in stabilizing the lean gas phase combustion. This is apparent from that flame at lean fuel conditions easily blows out in the absence of catalysts. A stable fuel-lean combustion can be successfully attained by employing the oxidation catalysts, of which surface reactions provide the heat necessary for the ignition and the progress of the gas-phase combustion below the flame temperature. This is the reason why the catalytic combustor can maintain peak temperatures well below the flame tempearture.

Figure 1.1 shows that thermal NO_x formation takes place as the combustion process proceeds, moving from the combustor inlet toward the outlet. The conventional combustor produces the peak temperature, which is far into the thermal NO_x formation region. The formation of thermal NO_x from N_2/O_2 mixture can be expressed by the Zeldovich mechanism, in which the formation rate is basically controlled by the following reaction.[18-20]

$$N_2 + O \rightarrow NO + N \quad 7.6 \times 10^{13} \exp(-75500/RT) \quad (R:cal/mol, T/K)$$
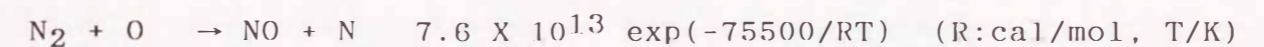
The high activation energy of this reaction leads to the strong temperature dependence of the NO_x formation. This means that the combustion temperature is preferred to be as low as possible in order to reduce NO_x emissions.

Emission performance of the catalytic combustor is schematically shown in Fig. 1.3.[18-20] Although in a conventional flame combustor, much of attempt has been done for the reduction of emissions by utilizing a lean, premixed, prevaporized combustion, these combustor designs suffer from unstable combustion and resultant drop in the combustion temperature leads to significant CO emission. On the contrary, thermal NO_x and CO can be significantly reduced simultaneously by using the catalytic combustor. The primary reason that catalytic combustors can reduce thermal NO_x formation without increasing CO emission is due to their capability to carry out stable, highly efficient combustion of lean fuel mixtures. This is effective in suppressing the peak temperature below the temperature at which appreciable amounts of NO_x formation occur (Fig. 1.1).
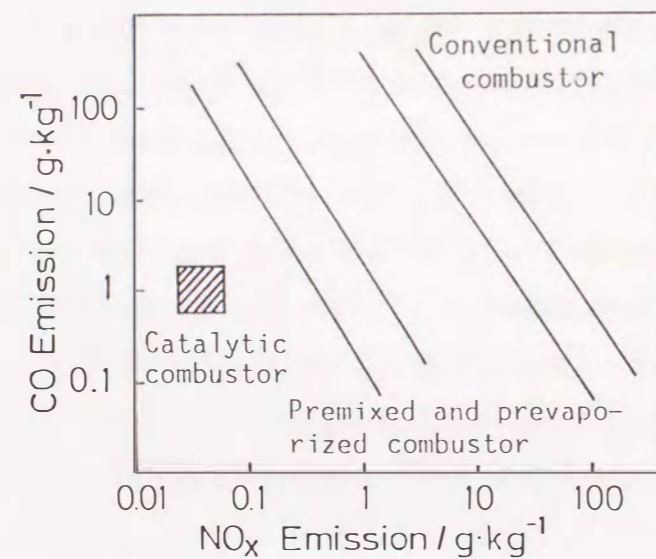
Fig. 1.3.   CO and NO_x emission of different combustion systems.

1.1.2 Catalytic Materials

The combustion catalysts operated above 1200 ℃ require the high heat resistance as well as the combustion activity. Even though this means that the catalyst properties necessary for catalytic combustion are quite different from those for conventional oxidation catalysts, the catalyst design from such a viewpoint has not been examined so far.   Materials required for high-temperature combustion are summarized in this section.

a) Substrate and support materials

Combustion catalysts are generally comprised of an active species, a oxide support (washcoat), and a substrate. Substrates are shaped into monolithic honeycomb structure in order to reduce a back pressure. The most common heat resistant substrate based on alumina, which is inexpensive and can be operated at high temperature (>1480 ℃). Zirconia can be used at higher tempera-

ture up to 2210 ℃ without any interaction with metals. Cordierite is most widely used honeycomb ceramics with the highest thermal shock resistance. However, the low melting point will limit the operation temperature below 1300 ℃.   For higher temperature and lower thermal expansion, aluminium titanate ceramics are studied.

Support and/or washcoat oxides serve important functions even in the catalytic combustion. One of the crucial problem is to suppress sintering and to retain large surface area of the oxide supports.[21,22] For transition aluminas, which are the most commonly used support material, their transformation to α-phase accompanies the significant loss in surface area (ca. 100 m^2/g at 1100 ℃ to 2 m^2/g at 1300 ℃). Thermal stabilization of alumina by additives has been reported by several researchers as summarized in Table 1.1.[23-35] These effects are originated from the inhibition of the phase transformation to α-phase and/or the sintering of metastable phase, which cause significant loss in surface area above 1000 ℃. Lanthanum oxide, which is the best-known inhibitor against the sintering of transition aluminas,[24-33] produces a surface layer identified as $LaAlO_3$.[28] Such a surface layer inhibits the surface diffusion of transition aluminas or corundum nucleation in the initial step of the phase transformation to α-phase. Addition of SiO_2 also produces surface compounds or glassy layers, which prevent the phase transformation. [24,25] Other additives, such as Li^+, K^+, and Ba^{2+}, are considered to suppress an atomic diffusion by occupying a certain lattice site.[23,24] Consequently, the role of these additives is to suppress the sintering of alumina kinetically. However, it appears doubtful that these mechanisms are effective above 1200 ℃, because these alumina-additive systems are in a metastable state.

A different type of the stabilization was reported by Matsu-da et al.[34] They suggested that the addition of La_2O_3 to alumina resulted in the formation of La·β-alumina, which retains the large surface area of ca. 30 m^2/g after calcination at 1200 ℃. Other rare earth elements, Pr and Nd, which produce β-alumina structure also stabilized the surface area of alumina.[35] Since these compounds are the equilibrium crystal phases, their thermal stability is expected to exceed that of the conventional addi-tive-alumina systems mentioned above.

Table 1.1 Improvement of thermal stability of transition alumina by additives

Additives	Atomic fraction	Location occupied by additives	Stabilization mechanism (Inhibited process)	Max. Temp.	Ref.
Li$^+$	< 2%	Lattice Al^{3+} vacancy	Bulk Al^{3+} diffusion	1000 ℃	23
K$^+$	< 3%	Surface site	Surface diffusion	1000 ℃	23
Mg^{2+}	< 3%	Deposition in pores	–	1000 ℃	23
Ba^{2+}	–	Lattice Al^{3+} site	Bulk Al^{3+} diffusion	1200 ℃	24
Si^{4+}	–	Glassy surface layer	γ-α transformation	1200 ℃	24
Si^{4+}	3wt%(Si)	Surface layer	Interaction with vapor water	1220 ℃	25
La^{3+}	1%	Surface compound	Surface diffusion	1100 ℃	26-28
Ln^{3+} (Ln=La,Pr,Nd)	1%	Surface LnAlO$_3$ phase	Corundum nucleation	1150 ℃	27
La^{3+}	3wt%(La)	Surface layer	–	910 ℃	30,31
La^{3+},Th^{4+} Zr^{4+},Ca^{2+}	1%	Lattice Al^{3+} site or cation vacancy	γ-α transformation	1150 ℃	32,33
Ln^{3+} (Ln=La,Pr,Nd)	5%	Formation of LnAl$_{11}$O$_{18}$	–	1400 ℃	34,35

b) Active components

Noble metals

Noble metals possess the highest catalytic activity and thus initiate the catalytic oxidation of fuels at the lowest possible temperatures.[36-38] From a practical view point, however, the use of noble metals in a combustor should be limited because of the following two serious problems. One is due to the high volatility of noble metals or their oxides at high temperatures. Except for Pd, the vapor pressure of the oxide is much higher than those of metallic state.[39] Since these noble metals are used as highly dispersed fine particles and exposed to gas of high velocity, volatilization will proceed more rapidly. Previous studies indi-cate that noble metals other than Pt and Pd can be hardly used for catalytic combustion. Palladium is the most possible active spe-cies for catalytic combustion below 1000 ℃. The interaction between PdO and alumina surface is sufficient to give considerable thermal stability.[40-42]

The other problem of noble metals is the ease of sintering at relatively low temperatures (500-900 ℃). Sintering results in a loss of the active surface area and hence in the reduction of relative catalytic activity. Therefore, a large particle (<10μm) Pd catalyst is examined for stable operation of combustors.[43] Some additives such as MgO were reported to inhibit the fusion of dispersed Pd particles.[44] Similar effects were obtained by the interaction between noble metals and support materials. In order to prevent the deterioration of catalysts due to the sintering, heat resistance should be much more improved not only for active species but also for support oxides.

Metal oxides and mixed oxides

A great deal of fundamental and industrial study on catalytic oxidation over various metal oxide systems was reported so far.[45-48] The relation between the catalytic activity and the physicochemical properties of metal oxides is systematically understood as the reduction-oxidation model with the volcano-type relation.[49-51] Some of these oxide catalysts, e.g., perovskite type oxides containing Mn or Co cations,[52-53] can substitute for the noble metals as practical oxidation catalysts at low temperatures. However, only few study was reported concerning the catalyst design emphasizing on the heat resistance which is the most advantaged character of oxides.

It was reported that the metallorganic-aided preparation procedure such as an amorphous citrate process[54] is quite effective in producing a large surface area (ca.30 m^2/g) of perovskite oxides as well as other single oxides at low temperatures.[55] But these oxide catalysts easily sinter into a large grain with low surface areas (< 1 m^2/g) above 1000 ℃ regardless of preparation procedures. Thus, how to stabilize the active phase by supporting on the thermally stable oxides (hexaaluminate-related compounds[56] and ZrO_2[57]) is interested. In the supported oxide system, however, a more serious problem is how to suppress the solid state reaction between the catalyst and the oxide support at high temperatures.

1.2 Outline of the Thesis

As pointed out in the above mentioned short review of catalytic combustion, the development of heat resistant catalyst materials is a valuable and urgent study for the practical application. Such a need for thermally stable catalysts is not limited to catalytic combustion. General high-temperature catalytic processes, e.g., steam reforming, automobile, and other emission gas control also suffer from thermal deactivation of conventional catalyst materials. However, there is no doubt that heat resistance necessary for high-temperature catalytic combustion is the most difficult target, which could not be succeeded by the conventional catalyst design.

Here, thermal stability or heat resistance of catalysts means the retention of the large surface area and the high catalytic activity at high temperatures. Although the previous studies concerning solid catalysts revealed the improvement of thermal stability of some oxide supports, in particular, alumina, their heat resistance is not enough for the high-temperature combustion operated above 1200 ℃. More systematic knowledge is required to attain the large surface area and the high catalytic activity at such a temperature region. It must be pointed out that the development of heat resistant catalysts includes following serious difficulties from a view point of materials design. First, fine particles with a large surface area are apt to sinter into large agglomerates because of their large surface energy. Secondly, active catalysts are also apt to be thermally deactivated. Catalysts dissociate oxygen molecules and oxygen atoms (or ions) thus formed sometimes participate the mass transfer process which determines the rate of sintering. For catalytically active oxides, the lattice oxygen is so active that both bulk and surface diffusion will proceed rapidly to accelerate their sintering. How to solve these trade-off relations is a key to the successful design of combustion catalysts.

From the above stand points, this study has been directed toward the materials design of the heat resistant catalyst for

high temperature catalytic combustion. Two new design concepts of the high-temperature combustion catalyst are proposed here in this study to solve the trade-off mentioned above.

This study consists of two major parts.   In the first part (Chapters 2-4), the development of heat resistant fine particles and their characterization are described. This part begins with a material screening, in which an effect of additives on the surface area of various oxide supports was examined (Chapter 2). The results revealed that the surface area of alumina is always stabilized when the additives give rise to the formation of the hexaaluminate structure. For the hexaaluminate compounds, the key material for the solution of the first trade-off, the stabilizing effect is discussed and compared to the other type of alumina-additives systems reported previously.

Chapter 3 describes the preparation of large surface area hexaaluminates. Hydrolysis of metal alkoxides showed inherent advantages in deriving the largest surface area at elevated temperatures. Relation between the preparation method with different formation routes of hexaaluminate and the resultant surface area is discussed from the solid state reaction mechanism. The effect of hydrolysis conditions on the microstructure of hexaaluminate is also described.

In Chapter 4, crystallographic elucidation of the excellent heat resistance is examined from a view point of morphology, crystal growth, and solid state diffusion of hexaaluminate. High resolution electron microscopes and secondary ion microscope analysis employed here provided valuable information on structure-crystal growth relations.

In the second part (Chapters 5,6), the material design of high-temperature combustion catalysts is studied by using hexaa-

luminate as a base material. Toward the solution of the second trade-off between the catalytic activity and the sinterability, a new structural concept, in which active species are dispersed in the hexaaluminate lattice, is first proposed in Chapter 5. The incorporation of various metal elements was examined as the partial cation-substitution of hexaaluminate and as the subsequent structural modification. Moreover, catalytic properties of hexaaluminates are discussed in connection with the redox property of the incorporated elements.

Finally, the combustion activity of the hexaalumiante catalyst was evaluated under practical combustor conditions (Chapter 6). The heat resistance of the hexaaluminate catalyst is found to be very important for the high performance of combustion at high temperatures and at high space velocities of feed gas. It should be noted that the second part of this thesis describes a systematic study on catalytic properties of hexaaluminate for the first time.

At the last of the thesis, the results of the above investigations are summarized in Chapter 7.

References

1 M.Sadakata, Energy to Shigen, 11, 22 (1990).

2 H.Arai and M.Machida, Chemical Engineering, 36, 47 (1991).

3 H.Arai and M.Machida, Shokubai, 33, 328 (1991).

4 W.C.Pfefferle, ASME Paper #75-WA/FV-1, (1975).

5 W.C.Pfefferle, J.Energy, 2, 142 (1978).

6 J.P.Kesselring, in "Advanced Combustion Methods", London, Academic Press, 1986, pp.238.

7 Z.R.Ismagilov and M.A.Kerzhentsev, Catal. Rev. Sci. Eng.,32, 51 (1990).

8 H.Fukuzawa and Y.Ishihara, Energy to Shigen, 2, 424 (1981).

9 H.Arai, Hyoumen, 24, 658 (1986).

10 T.Ono and S.Ichihara, Shokubai, 29, 305 (1987).

11 T.Inui, Denki Kagaku, 57, 949 (1989).

12 T.Haruta, Denki Kagaku, 57, 951 (1989).

13 H.Arai and M.Machida, Energy to Shigen, 11, 228 (1990).

14 T.Ono, in "Shokubai Koza 9" Kodansha, Tokyo, 1985, pp.189.

15 W.S.Blazowski and D.E.Walsh, Combust. Sci. Technol., 10, 233 (1975).

16 D.N.Anderson, R.R.Tacina, and T.S.Mroz, NASA TM X-71747, June 1975.

17 S.M.DeCorso, S.Mumford, R.V.Carrubba, R.Heck, ASME Paper No.76-GT-4,159, (1977).

18 D.L.Trimm, Appl. Catal., 7, 249 (1983).

19 R.Prasad, L.A.Kennedy, and E.Ruckenstein, Catal. Rev., 26, 1 (1984).

20 L.D.Pfefferle and W.C.Pfefferle, Catal. Rev., 29, 219 (1987).

21 S.Matsuda and H.Yamashita, Shokubai, 29, 305 (1988).

22 M.Machida and H.Arai, Fine Ceramics, 45, 175 (1989).

23 R.M.Revy and D.J.Bauer, J. Catal., 9, 76 (1967).

24 I.Amato,D.Martorama, and B.Sliengo,"Sintering and Catalysis," p.187, ed by G.C.Kuczunski, Plenum Press, New York and London (1975).

25 B.Beguin, E.Garbowski, and M.Primet, J. Catal., 127, 595 (1991).

26 H.Schaper, E.B.M.Doesburg, and L.L.Van Reijan, Appl. Catal., 7, 211 (1983).

27 H.Schaper, D.J.Amesz, E.B.M.Doesburg, and L.L.Van Reijan, Appl. Catal., 9, 129 (1983).

28 H.Schaper, E.B.M.Doesburg, P.H.M.DeKorte, and L.L.Van Reijan, Solid State Ionics, 16, 261 (1985).

29 F.Oudet, P.Courtine, and A.Vejux, J. Catal.,114, 112 (1988).

30 F.Oudet, A.Vejux, and P.Courtine, Appl. Catal.,50, 79 (1989).

31 M.Bettman, R.E.Chase, K.Otto, and W.H.Weber, J. Catal.,117, 447 (1989).

32 P.Burtin, J.P.Brunelle, M.Pijolat, and M.Soustelle, Appl. Catal.,34, 225 (1987).

33 P.Burtin, J.P.Brunelle, M.Pijolat, and M.Soustelle, Appl. Catal.,34, 239 (1987).

34 S.Matsuda, A.Kato, M.Mizumoto, and H.Yamashita, Proc. 8th Int. Congress on Catal., Berlin, 1984, Vol.4, p.879, Dechama, Frankfurt.

35 S.Matsuda, Seramikkusu, 20, 189 (1985).

36 H.Yamashita, A.Kato, N.Watanabe, and S.Matsuda, Nippon Kagaku kaishi, 1986, 1169 (1986).

37 G.J.K.Acres, Platinum Met, Rev.,14, 2 (1970).

38 A.Shwartz, L.L.Holbrook, and H.Wise, J.Catal., 21, 199 (1971).

39 M.A.Quinlan, H.Wise, and J.G.McCarty, SRI Project PYH-1887 (1989).

40 H.H.Lee and E.Ruckenstein, Catal. Rev., 25, 475 (1983).

41 E.Ruckenstein and D.B.Dadyburjor, Rev. Chem. Eng.,1, 251 (1983)

42 R.L.Klimisch J.C.Summers, and J.C.Schlatter, Adv. Chem. Ser., 1975, 143 (1975).

43 K.Yonehara and K.Tsutiya, Nippon Tokkyo Koho 88 66258.

44 T.Hayata, T.Furuya, S.Yamanaka, and J.Koizuka, Shokubai, 31, 116 (1989).

45 R.Prasad, L.A.Kennedy,and E.Ruckenstein, Combust. Sci. Tech.,22, 271(1980).

46 H.Tong, G.C.Show, E.K.Chu, R.L.S.Chamg, M.J.Angwin, and S.L.Pessagno, NASA CR-165396, September 1981.

47 J.P.Kesselring, W.V.Krill, H.L.Atkins, R.M.Kendoll, R.M.Kelley, and J.T. Kelly, EPA-600/7-79-181, August 1979.

48 R.Prasad, H.L.Tsai, L.A.Kennedy,and E.Ruckenstein, Combust. Sci. Technol., 26, 51 (1980).

49 A.A.Baladine, in "Advances in Catalysis," ed by D.D.Eley, H.Pines, and P.B. Weisz, Vol. 10, p.95, Academic Press, New York, 1958.

50 Y.Morooka and A.Ozaki, J. Catal., 5, 116 (1966).

51 S.Kagawa, Y.Kajiwara, S.Tokunaga, and T.Seiyama, Shokubai, 8, 306 (1966).

52 T.Nakamura, M.Misono, T.Uchijima, and Y.Yoneda, Nippon Kagaku Kaishi, 1980, 1679 (1980).

53 H.Arai, T.Yamada, K.Eguchi, and T.Seiyama, Appl. Catal.,26, 265 (1986).

54 D.J.Anderton and F.R.Sale, Powder Metal., 1971, 14 (1971).

55 H.Zhang, Y.Teraoka, and N.Yamazoe, Chem. Lett., 1987, 665 (1987).

56 H.Zhang, Y.Teraoka, and N.Yamazoe, Appl. Catal., 41, 137 (1988).

57 N.Mizuno, H.Fujii, and M.Misono, Chem. Lett., 1986, 1333 (1986).

Chapter 2

EFFECT OF ADDITIVES ON SURFACE AREA OF OXIDE SUPPORT

2.1 Introduction

Practical applications of catalytic combustion require the design of a new catalyst system because conventional catalysts are deactivated due to sintering and/or vaporization.[1-3] Maintaining the surface area of oxide supports is one of the most important problems for the industrial application of high-temperature catalytic combustion. Most of fuel molecules are almost completely oxidized for such purposes but complete combustion of fuels at a high conversion level is strongly affected by the mass transfer of reactants to the active surface from gas phase rather than the activity of each active sites. The catalytic activity at the high conversion region is almost determined by the area of the reaction surface.

Although alumina is widely used as an oxide support, its surface area significantly decreases simultaneously with the transition from metastable phases into α-phase. Some attempts have been made to design oxide supports, but few materials satisfy both high heat resistance and a large surface area at high temperatures of interest. The effect of additives such as BaO, La_2O_3, MgO, Li_2O, K_2O and SiO_2 on the surface area of alumina was reported by several researchers as mentioned in Chapter 1. These additives are effective in suppressing the phase transformation accompanied by significant sintering, but the details were not studied as to use them for support materials for high temperature

combustion operated above 1200 ℃.

In this chapter, the effect of additives on the surface area of Al_2O_3-, ZrO_2- and MgO-based oxides was examined. Since the $BaO-Al_2O_3$ system was revealed to have the largest surface area in the material screening, the relation between the crystal phase and the thermal stability was studied in detail.

2.2 Experimental
2.2.1 Preparation of Samples

Metal oxide and carbonate ($MgCO_3$, $CaCO_3$, $SrCO_3$ and $BaCO_3$) powders were used as starting materials for oxide supports. γ-alumina was used for the preparation of alumina-based support oxides. Powder mixtures of oxides and/or carbonates were calcined at 1450 ℃ for 5 h in air. Crystal structures of samples were determined by the powder X-ray diffraction (Rigaku Denki 4011) with Cu $K\alpha$ radiation. Specific surface area of oxide supports was measured by the BET method using nitrogen adsorption.

Cobalt oxide was selected as an active component for combustion of methane and was supported by a conventional impregnation method. Support oxides were suspended in an aqueous solution of cobalt nitrate followed by evaporation to dryness. Dried samples were calcined at 1300 ℃ prior to use in the combustion reaction. The loading amount of cobalt oxide was 10wt% as CoO.

2.2.2 Catalytic Reaction

Catalytic activity for methane combustion was measured in a conventional flow system at atmospheric pressure. Catalysts were fixed in a quartz reactor by packing alumina beads at both ends of the catalyst bed. A gaseous mixture of methane (1 vol%) and air (99 vol%) was fed to the catalyst bed at a flow rate of

48000 cm^3/h (space velocity=48000 h^{-1}). The methane conversion in the effluent gas was analyzed by on-line gas chromatography. Catalytic activity was evaluated in terms of the temperature at which conversion level attains 90% and denoted as $T_{90\%}$. Thus, the small value of $T_{90\%}$ indicates correspondingly high catalytic activity. These values were estimated from the temperature dependence of the methane conversion to carbon dioxide.

2.3 Surface Area of Oxide Support and Effect of Additives

Surface area of oxide supports at high temperatures is dependent on their intrinsic properties (melting point and phase transformation) and is also influenced by some extrinsic factors (water vapor pressure, oxygen pressure, and impurities) as well. MgO and ZrO_2, for instance, offer high melting points above 2500 ℃ so that the surface area is stable even at the operation temperatures of combustors. Magnesia can retain the largest surface area among the single oxides examined here because of the extremely high melting point (2852 ℃). Phase transformation, which activates atomic diffusion, sometimes results in significant sintering as can be seen in the case of Al_2O_3 ($\gamma-\alpha$, ca. 1100 ℃) and in TiO_2 (anatase-rutile, ca.700 ℃).

The effect of additives on the surface area of these oxides was studied.[4,5] Surface areas of Al_2O_3-, ZrO_2-, and MgO-based oxides containing 10 mol% of additives were measured after calcination at 1450 ℃ (Table 2.1). The effect of additives was scarcely observed or was observed as a slight decrease in surface area for MgO- and ZrO_2-based oxides. Although the surface areas of pure and MgO-, and ZrO_2-added alumina were less than 1.5 m^2/g after calcination at 1450 ℃, BaO-added alumina, i.e., $(BaO)_{0.1}$-$(Al_2O_3)_{0.9}$. showed the three times larger surface area. It seems

Table 2.1 Surface area of oxide supports and catalytic activities of supported cobalt oxide catalysts for methane combustion

Support	Surface area[a] /m^2g^{-1}	$T_{90\%}$[b,c] / ℃	Crystal phase[d]
Al_2O_3	1.4	–	$\alpha-Al_2O_3$
$(BaO)_{0.1}(Al_2O_3)_{0.9}$	4.5	790	$\alpha-Al_2O_3+BaAl_{12}O_{19}$
$(MgO)_{0.1}(Al_2O_3)_{0.9}$	1.2	820	$\alpha-Al_2O_3+MgAl_2O_4$
$(ZrO_2)_{0.1}(Al_2O_3)_{0.9}$	1.0	810	$\alpha-Al_2O_3+ZrO_2(ss)$
ZrO_2	0.8	–	ZrO_2
$(MgO)_{0.1}(ZrO_2)_{0.9}$	0.3	860	$ZrO_2(ss)$
$(CaO)_{0.1}(ZrO_2)_{0.9}$	0.9	820	$ZrO_2(ss)$
$(Al_2O_3)_{0.1}(ZrO_2)_{0.9}$	0.5	845	$ZrO_2(ss)$
MgO	9.6	–	MgO
$(Al_2O_3)_{0.1}(MgO)_{0.9}$	1.0	820	$MgO+MgAl_2O_4$
$(SiO_2)_{0.1}(MgO)_{0.9}$	1.3	840	$MgO+Mg_2SiO_4$
$(Cr_2O_3)_{0.1}(MgO)_{0.9}$	1.5	825	$MgO+MgCr_2O_4$

a Calcined at 1450 ℃.
b Temperature at which conversion level is 90%.
c Loading of CoO, 10wt%. Reaction conditions; CH_4 1 vol%, air 99 vol%, S.V.=48000 h^{-1}.
d 'ss' means solid solution.

Table 2.2 Surface area of alkaline earth metal aluminates and catalytic activities of supported cobalt oxide catalysts for methane combustion

Support	Surface area[a] /m^2g^{-1}	$T_{90\%}$[b,c] / ℃	Crystal Phase
Al_2O_3	1.4	–	$\alpha-Al_2O_3$
$(BaO)_{0.14}(Al_2O_3)_{0.86}$	6.0	760	$BaAl_{12}O_{19}$
$(SrO)_{0.14}(Al_2O_3)_{0.86}$	4.2	765	$SrAl_{12}O_{19}$
$(CaO)_{0.14}(Al_2O_3)_{0.86}$	5.0	755	$CaAl_{12}O_{19}$
$(MgO)_{0.10}(Al_2O_3)_{0.90}$	1.2	820	$\alpha-Al_2O_3+MgAl_2O_4$

a Calcined at 1450 ℃.
b Temperature at which conversion level is 90%.
c Loading of CoO, 10wt%. Reaction conditions; CH_4 1 vol%, air 99 vol%, S.V.=48000 h^{-1}.

that the addition of barium oxide suppressed the sintering of alumina and retained the larger surface area at high temperatures.

Oxidation of methane over cobalt oxide catalysts was carried out using the oxide supports thus prepared. The catalytic activities of supported cobalt oxide catalysts are also summarized in Table 2.1. It is noted that activities, which are expressed by $T_{90\%}$, roughly depend on the surface area of support materials. Most of the catalysts attained $T_{90\%}$ of conversion level only above 800 °C. In this temperature region, methane is oxidized by homogeneous gas phase reaction by passing through the catalyst bed. However, cobalt oxide supported on $(BaO)_{0.1}(Al_2O_3)_{0.9}$ with the largest surface area showed the relatively high activity.

Series of alkaline earth metal oxides were also mixed with alumina and the effect on surface area was investigated (Table 2.2). The addition of SrO and CaO to alumina also brought about a large surface area as in the $BaO-Al_2O_3$ system. Moreover, the crystalline phase denoted as $MAl_{12}O_{19}$ (M=Sr, Ca) of these systems is similar to that of the $BaO-Al_2O_3$ system. The methane oxidation activity indicated that the catalysts supported on BaO-, SrO- and CaO-added alumina were more active than that supported on alumina and $MgO-Al_2O_3$. Thus, the large surface area should be quite effective in enhancing the combustion activity. Further study was focused on the $BaO-Al_2O_3$ system to elucidate the origin of the large surface area.

2.4 Crystal Phase and Surface Area of $BaO-Al_2O_3$ System

The barium oxide-alumina system exhibits the largest surface area and is most promising for a support material for high temperature catalytic combustion. In this section, the reported phase diagram and the crystal structures of this system are briefly described for the later discussion. The molar fraction of BaO in binary oxides is expressed by x in $(BaO)_x(Al_2O_3)_{1-x}$. Equilibrium phases appeared in the phase diagram of the $BaO-Al_2O_3$ system were reported by Purt et al.[6] (Fig. 2.1) α-Phase is the equilibrium phase of pure alumina. Two binary compounds, i.e., $BaAl_{12}O_{19}$ (x=0.14) and $BaAl_2O_4$ (x=0.5), are known in the composition range from x=0 to x=0.5. The oxide except for these two composition are the mixtures of $BaAl_{12}O_{19}$ and $BaAl_2O_4$ or $\alpha-Al_2O_3$ and $BaAl_{12}O_{19}$.

Crystallographic analysis indicated that barium hexaaluminate, $BaAl_{12}O_{19}$, is a pseudo-layered structure, which can be classified into two types of related structures as shown in Fig. 2.2.[7-11] The structure of equimolar compounds, $BaAl_2O_4$, is called a stuffed trydimite type. The atomic arrangement in this structure is represented by completely replacing the Si^{4+} site in the trydimite lattice with Al^{3+} ions. Because of the charge neutrality requirement, barium ions are placed at the large hole in the framework of AlO_4 tetrahedra.[12,13]

X-Ray diffraction patterns and surface area of the barium oxide-alumina system with various composition ratios were measured after heating at 1450 °C. Figure 2.3 shows the X-ray diffraction patterns of $(BaO)_x(Al_2O_3)_{1-x}$. All of the diffraction peaks from pure alumina are ascribable to α-phase. The diffraction patterns of oxides at x=0.14 and 0.5 consisted of single phases of $BaAl_{12}O_{19}$ and $BaAl_2O_4$, respectively. Samples between these compositions are mixtures of $\alpha-Al_2O_3$ and $BaAl_{12}O_{19}$ at 0<x<0.14 and of $BaAl_{12}O_{19}$ and $BaAl_2O_4$ at 0.14<x<0.5. Thus, the results of X-ray diffraction confirms that samples consisted of the equilibrium phases after calcination at 1450 °C.
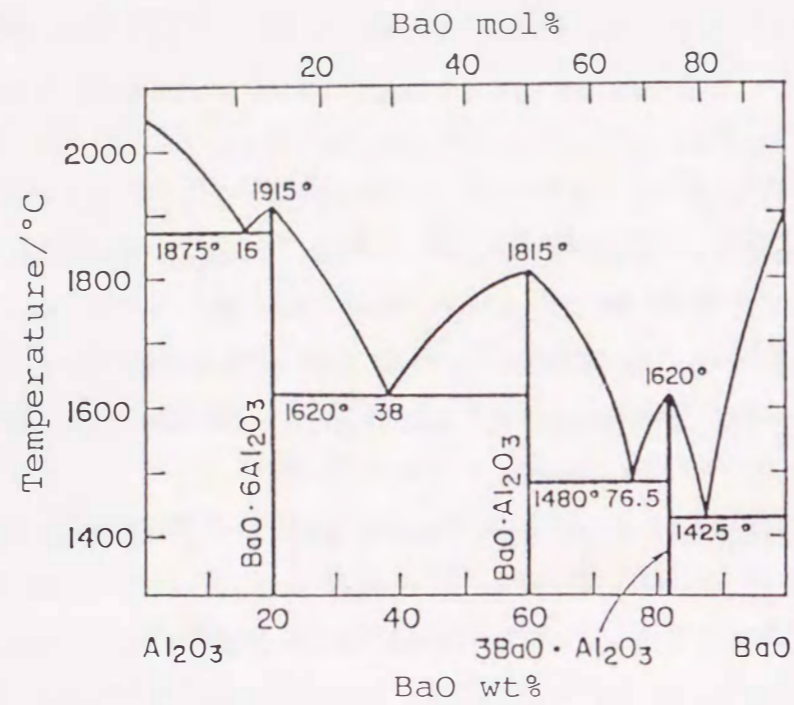
Fig. 2.1.   Phase diagram of BaO-Al$_2$O$_3$ system reported by Purt.[6]

Mirror plane

Spinel block

Mirror plane

Magnetoplumbite   ß-Alumina
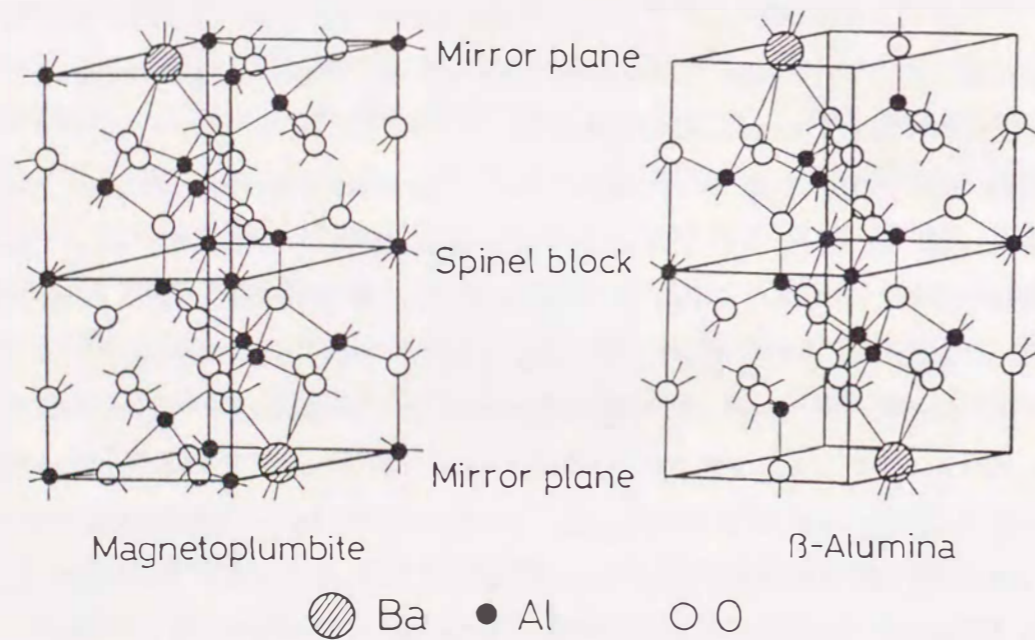
Ba   • Al   ○ O

Fig. 2.2.   Crystal structure of hexaaluminate structure.
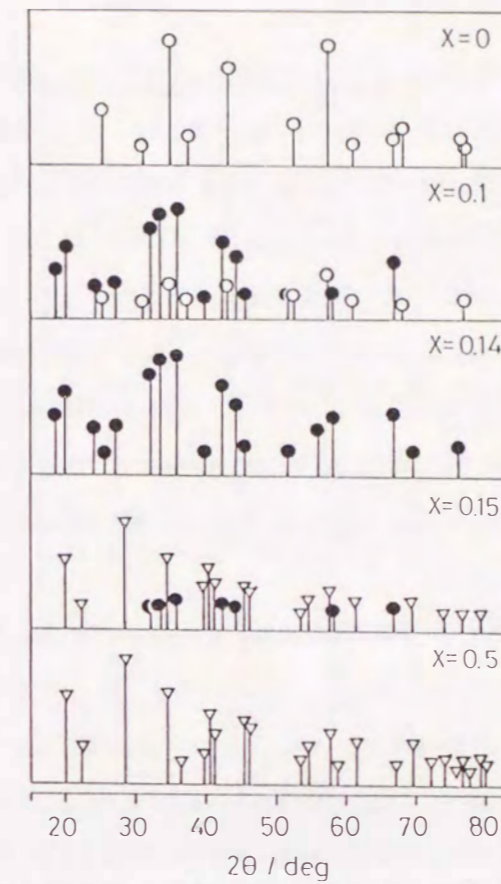
Fig. 2.3.   X-Ray diffraction patterns of $(BaO)_x(Al_2O_3)_{1-x}$ system
calcined at 1450 ℃.
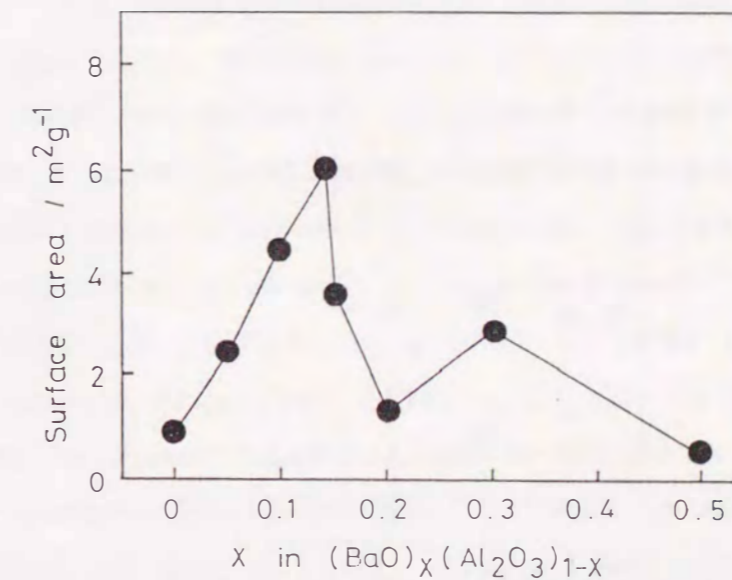○ α-Al$_2$O$_3$,   ●   BaAl$_{12}$O$_{19}$,   ▽   BaAl$_2$O$_4$

Fig. 2.4.   Surface area of $(BaO)_x(Al_2O_3)_{1-x}$ system after calcina-
tion at 1450 ℃.

The surface area of $(BaO)_x(Al_2O_3)_{1-x}$ after heating at 1450 °C is plotted as a function of x in Fig. 2.4. It is clearly shown that the surface area increased with the addition of barium oxide to alumina up to the maximum value of 6.0 m^2/g at x=0.14. Then, it decreased gradually with a further increase in barium oxide content at 0.14<x<0.5. The composition at the maximum surface area agreed closely with that of barium hexaaluminate, indicating that the formation of this binary compound suppressed the decrease in surface area during the heating process.

2.5 Effect of Hexaaluminate Formation on Surface Area

Detailed investigations were focused on the sample at x = 0.14, which showed the largest surface area in the $BaO-Al_2O_3$ system. Figure 2.5 shows the X-ray diffraction patterns of $(BaO)_{0.14}(Al_2O_3)_{0.86}$ during the course of heating. It is noted that the binary compound produced at the first stage of the solid state reaction was not the equilibrium phase, but $BaAl_2O_4$ with a trace amount of $BaCO_3$. The equilibrium phase, i.e., $BaAl_{12}O_{19}$, appeared only after heating above 1200 °C. The sample finally consisted of a single $BaAl_{12}O_{19}$ phase above 1450 °C with the completion of the solid state reaction. Such a complicated reaction is typical for the powder mixture process. Detail formation processes of hexaaluminate is discussed in Chapter 3.

The surface area of $(BaO)_{0.14}(Al_2O_3)_{0.86}$ in the heating course is shown in Fig. 2.6 with reference to pure alumina. Although both samples had almost the same amount of surface area after calcination at 1000 °C, significant decreases followed a rise in calcination temperature. The decrease was more steep for Al_2O_3 than for $(BaO)_{0.14}(Al_2O_3)_{0.86}$. The steep decrease in surface area of alumina was accompanied by the phase transition

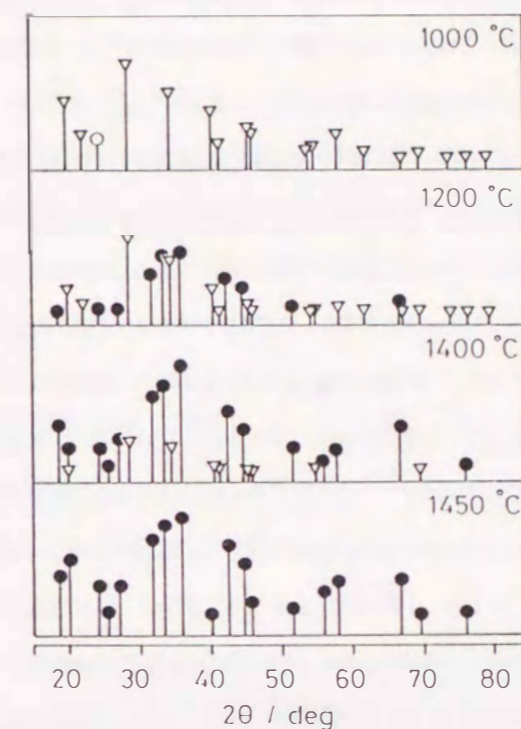Fig. 2.5. X-Ray diffraction patterns of $(BaO)_{0.14}(Al_2O_3)_{0.86}$ calcined at various temperatures.
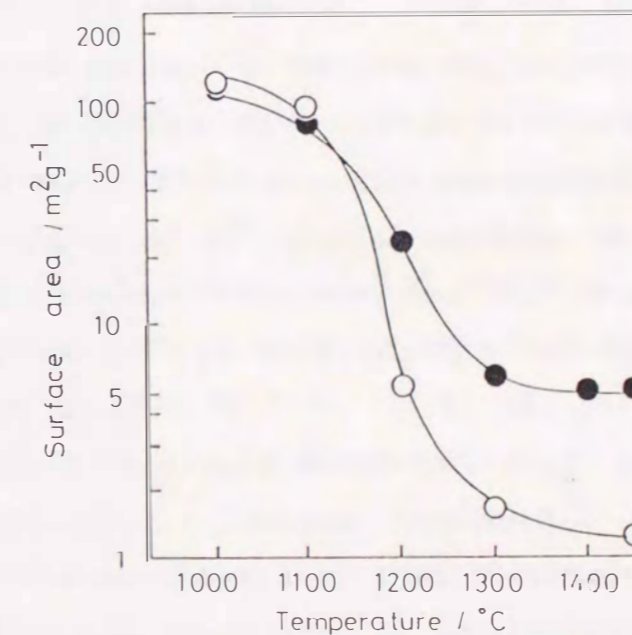● $BaAl_{12}O_{19}$, ▽ $BaAl_2O_4$, ○ $BaCO_3$

Fig. 2.6. Surface area of $(BaO)_{0.14}(Al_2O_3)_{0.86}$ calcined at various temperatures.
● $(BaO)_{0.14}(Al_2O_3)_{0.86}$ ○ Al_2O_3

to α-phase.   In   the case of $(BaO)_{0.14}(Al_2O_3)_{0.86}$, however, the decrease of surface area was suppressed with correspondence to the formation of barium hexaaluminate.

These results indicate that the large surface area of BaO-Al_2O_3 system appears to originate from the formation of barium hexaaluminate. The large surface area could be obtained by an addition of CaO and SrO, which also produced the hexaaluminate structure (Table 2.2) in agreement with reported phase diagram.[14-16] However, their effects were not so strong as that of barium oxide. Although three alkaline earth oxides, i.e., CaO, SrO, BaO, are more or less effectively enhanced the surface area at elevated temperature, an addition of MgO to alumina leads to a decrease in surface area.   While a spinel phase is known as the equilibrium phase for the MgO-Al_2O_3 system, magnetoplumbite and other layered aluminate structures are not formed because of the small ionic radius of Mg^{2+}.

2.6 Comparison with Other Alumina-Additive Systems

Sintering of alumina proceeds via bulk diffusion or surface diffusion. Also, the phase transformation to α-phase requires a change in the oxide ion lattice from cubic to hexagonal close packing and results in a full recrystallization with a significant loss in surface area. As mentioned in Chapter 1, several researchers have reported the effect of additives on the surface area of alumina.[17-25] Additives or impurities have a great influences on the sintering of alumina, not only stabilizing transition aluminas but also preventing $\gamma - \alpha$ transformation as summarized in Table 1.1.   While these effects could not be formulated at this moment, they must be closely related to the inhibition of the solid state diffusion on a surface or in a bulk, which

play a mass transport required in sintering of transition aluminas. However, the thermal stability of these additive-alumina systems in a metastable state is not enough for the use at combustion operation temperatures above 1300 ℃.

On the other hand, the formation of barium hexaaluminate as well as other alkaline earth hexaaluminates stabilize the surface area in the higher temperature range (1200-1600 ℃). Moreover, such an effect is quite similar to rare earth・β-alumina reported by Matsuda et al.[26-28] These compounds are similar to barium hexaaluminate except for a slight difference in the number of coordination cations as mentioned in an earlier section. Besides these di- or trivalent large elements, monovalent elements, such as potassium, also showed the same effect as revealed in the later part of this study. Therefore, it is concluded that the a large surface area can be obtained when the layered aluminate structure of magnetoplumbite or β-alumina (Fig. 2.2) is produced. Since the hexaaluminate compounds are equilibrium crystal phases at each compositions, thermal stability higher than that of any conventional alumina-additive systems must be available. Oxides which crystallize in other structures by mixing with alumina exhibited no effect or a decreasing effect on the surface area on the heating above 1200 ℃. This indicates that the large surface area is the structure-dependent property of hexaaluminates. The relation between the crystal structure and the large surface area retention is discussed in detail in Chapter 4.

2.7 Conclusion

This Chapter indicated that the barium oxide-alumina system, which maintains the large surface area at elevated temperatures, is quite appropriate as a thermally stable oxide support. When an

addition of oxides leads to the formation of a layered hexaalumi-
nate structure, the surface area is always higher than that of
pure alumina above 1200 ℃. The formation of barium hexaaluminate
exhibited the most outstanding effect in suppressing the decrease
in surface area. Catalytic activity for methane combustion
strongly depends on the surface area of support materials. Since
the large surface area of support materials always gives rise to
an enhanced catalytic activity at a high conversion level, choice
of support materials is very important for combustion catalysts.
Hexaaluminate compounds are likely to prove extremely useful in
catalytic combustion.

References

1 D.L.Trimm, Appl. Catal.,7, 249 (1983).
2 R.Prasad, L.A.Kennedy, and E.Ruckenstein, Catal. Rev. Eng. Sci.,26, 1
  (1984).
3 D.J.Young and P.Udaja, and D.L.Trimm,in "Catalyst Deactivation," p.331,
  Elsevior, New York 1980.
4 M.Machida, K.Eguchi, and H.Arai, Chem. Lett., 1986, 151 (1986).
5 M.Machida, K.Eguchi, and H.Arai, J. Catal., 103, 385 (1987).
6 E.M.Levin, C.R.Robbins, H.F.McMurdie, "Phase Diagram for Ceramist," Fig.
  206, Am. Ceram. Soc., Columbus, 1964.
7 A.L.N.Steevels, and A.D.M.Schrama-de Pauw, J.Electrochem. Soc., 125, 691
  (1976).
8 J.M.P.J.Verstegen and A.L.N.Stevels, J. Lumin.,9, 406 (1974).
9 A.L.N.Stevels and A.D.M.Schrama-de Pauw, J. Electrochem.,123, 691 (1976).
10 S.Kimura E.Bannai, and I.Shindo, Mat. Res. Bull.,17, 209 (1982).
11 N.Iyi, S.Takekawa, Y.Bando and S.Kimura, J. Solid State Chem., 47, 34
   (1983).
12 A.J.Plotta and J.V.Smith, Bull. Soc. France Mineral Crystallogr., 91, 85
   (1968).
13 F.P.Glasser and L.S. Dent Glasser, J. Am. Ceram. Soc., 48, 377 (1963).
14 E.M.Levin, C.R.Robbins, H.F.McMurdie, "Phase Diagram for Ceramist," Fig.
   231, Am. Ceram. Soc., Columbus, 1964.
15 E.M.Levin, C.R.Robbins, H.F.McMurdie, "Phase Diagram for Ceramist," Fig.
   294, Am. Ceram. Soc., Columbus, 1964.
16 E.M.Levin, C.R.Robbins, H.F.McMurdie, "Phase Diagram for Ceramist," Fig.
   4331, Am. Ceram. Soc., Columbus, 1975.
17 B.Beguin, E.Garbowski, and M.Primet, J. Catal., 127, 595 (1991).
18 H.Schaper, E.B.M.Doesburg, and L.L.Van Reijan, Appl. Catal., 7, 211 (1983).
19 H.Schaper, D.J.Amesz, E.B.M.Doesburg, and L.L.Van Reijan, Appl. Catal., 9,
   129 (1983).
20 H.Schaper, E.B.M.Doesburg, P.H.M.DeKorte, and L.L.Van Reijan, Solid State
   Ionics, 16, 261 (1985).
21 F.Oudet, P.Courtine, and A.Vejux, J. Catal.,114, 112 (1988).
22 F.Oudet, A.Vejux, and P.Courtine, Appl. Catal.,50, 79 (1989).
23 M.Bettman, R.E.Chase, K.Otto, and W.H.Weber, J. Catal.,117, 447 (1989).
24 P.Burtin, J.P.Brunelle, M.Pijolat, and M.Soustelle, Appl. Catal.,34, 225
   (1987).
25 P.Burtin, J.P.Brunelle, M.Pijolat, and M.Soustelle, Appl. Catal.,34, 239
   (1987).
26 S.Matsuda, A.Kato, M.Mizumoto, and H.Yamashita, Proc. 8th Int. Congress on
   Catal., Berlin, 1984, Vol.4, p.879, Dechama, Frankfurt.

27 S.Matsuda, Seramikkusu, 20, 189 (1985).

28 H.Yamashita, A.Kato, N.Watanabe, and S.Matsuda, Nippon Kagaku kaishi, 1986, 1169 (1986).

Chapter 3

PREPARATION OF LARGE SURFACE AREA HEXAALUMINATE FROM METAL ALKOXIDES

3.1 Introduction

In the preceding chapter, the addition of BaO was revealed to improve the thermal stability of alumina.   The effect of BaO strongly depends on the formation of hexaaluminate, $BaAl_{12}O_{19}$, of which surface area reached 6 m^2/g even after calcination at 1450 ℃. Further improvement of surface area requires the preparation of hexaaluminate fine powders to be examined, because the large surface area is originated from this crystal phase.

The surface area of ceramic powders is susceptible to preparation method, the alkoxide process being superior to conventional preparation from a powder mixture because of high purity, very fine primary particle, and uniform mixing of components.[1-8] This Chapter describes the marked elevation of high temperature surface area retention of $BaAl_{12}O_{19}$ by employing the preparation from metal alkoxides with various conditions. The powder characteristics of sol-gel prepared powders were compared with those from the conventional powder process.   Furthermore, to elucidate the reaction mechanism effective for the large surface area, microstructures, chemical compositions, and crystal structures at a nanometer level were studied by analytical electron microscopy (AEM).[9,10]   The dependence of the solid state reaction mechanism on the chemical homogeneity of precursors was examined from the viewpoint of microstructure and microchemistry.

3.2 Experimental

3.2.1 Preparation of Samples

Barium hexaaluminate ($BaAl_{12}O_{19}$) was prepared from mixtures of $BaCO_3$ and γ-Al_2O_3. The average crystallite size of $BaCO_3$ and γ-Al_2O_3 were 0.8 μm and 5 nm, respectively. They were mixed with an automatic mortar grinder for 2 h before firing. The mixture was heated in air at a constant rate of 5 deg/min and kept at a desired temperature for 5 h.

A sample with the same composition was prepared by hydrolysis of the corresponding metal alkoxides. Barium isopropoxide, $Ba(OC_3H_7)_2$, was prepared by the reaction between Ba metal and 2-propanol in N_2 stream at 80 ℃.[11]

$$Ba + 2 C_3H_7OH \rightarrow Ba(OC_3H_7)_2 + H_2 \qquad (1)$$
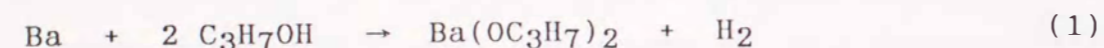
Calculated amounts of $Ba(OC_3H_7)_2$ and $Al(OC_3H_7)_3$ were dissolved together in 2-propanol and refluxed at 80 ℃ for 5 h with vigorous stirring. All the procedure before the hydrolysis has been carried out in a dried N_2 atmosphere. As distilled water was slowly added to the resulting clear solution, gelation was observed immediately accompanied by a rise in temperature from 80 to ca. 90 ℃. After several hours of aging under stirring at 80 ℃, the hydrolyzed alkoxides were evaporated to dryness in vacuo and the powders thus obtained were calcined in the above mentioned manner. Surface areas of alkoxide-derived $BaAl_{12}O_{19}$ were investigated as a function of the amount of water for hydrolysis and of an aging period of hydrolyzed alkoxides. Thus, a series hydrolysis reactions were performed in order to demonstrate the optimum preparation condition.

3.2.2 Characterization of Samples

Pore size distribution and BET surface areas of oxide powders were determined using nitrogen adsorption at 77 K. Crystal structures of the calcined samples were determined by X-ray diffraction (Rigaku Denki, 4011). Microstructures of the powder samples were measured by a scanning electron microscope (JEOL, JSM-50). Thermal decomposition of the hydrolyzed precursors to the corresponding oxides was observed by differential thermal analysis and thermal gravimetry (ULVAC, TGD 5000RH) in air. Samples were heated at a constant rate of 10 deg/min up to 600 ℃. The infrared spectra were taken on a JASCO IR810 spectrometer before and after the thermal decomposition. Mixtures of hydrolyzed precursors (30 mg) and KBr powders (300 mg) were pressed into disks of 20 mm in diameter and placed in a temperature-controlled in-situ cell. The infrared spectra were recorded after evacuation at elevated temperatures and subsequent cooling to room temperature.

3.2.3 Analytical Electron Microscopy

A JEM 2000FX electron microscope (HVEM Laboratory, Kyushu University) was used for imaging and selected area diffraction (SAD) in TEM mode operating at 200 kV. Local chemical compositions were obtained using a Tracor Northern TN2000 energy-dispersive X-ray spectrometer (EDS) with a beryllium window installed on the microscope. The electron probe (10-50 nm in diameter) was positioned at each location across a particle and the net Ba or Al X-ray counts (BaK_α and AlK_α) were measured. The Ba/Al ratio at each point was estimated from the X-ray counts. The analyses were performed at least 20 times for different particles heated at same temperatures.

3.3 Powder Properties of Alkoxide-Derived Hexaaluminate

γ-Alumina and the two BaO-Al_2O_3 precursors, which were prepared from powder mixtures and metal alkoxides, were heated at elevated temperatures for 5 h.   The decrease in surface area during the heat treatment was measured as a function of the calcination temperature (Fig. 3.1).   Surface areas of three samples are almost same after calcination at 1000 ℃, but their changes were in a different way with a rise in calcination tem-perature. The decrease in surface area was most significant in pure alumina. As revealed in Chapter 2, the addition of BaO was obviously effective in maintaining the surface area at higher temperatures because of the formation of $BaAl_{12}O_{19}$.   The surface areas of a typical alkoxide-derived sample are also shown in Fig. 3.1. It should be noted that the loss of surface area upon heat-ing was more gradual than that of the powder mixtures. Thus, the surface area of alkoxide-derived sample was 3 times larger than that from $BaCO_3$/γ-Al_2O_3 mixtures above 1300 ℃[12-14]. The value of 11 m^2/g after heating at 1600 ℃ has not been achieved by any oxide supports so far reported.

After calcination at 1450 ℃, microstucture of alumina and $BaAl_{12}O_{19}$ was observed by a scanning electron microscope (SEM), as shown in Fig. 3.2.   The particle size of alumina (ca.   2 μm) was considerably larger than that of the $BaAl_{12}O_{19}$ samples. Significant grain growth of alumina is evident from the large particles with a smooth surface. In contrast, the $BaAl_{12}O_{19}$ powder was clearly fine and possessed a rough surface.   The two $BaAl_{12}O_{19}$ samples are obviously different in their particle sizes and microstructures. When the mixture of $BaCO_3$ and γ-Al_2O_3 was calcined at 1450 ℃, the resultant particles (0.5-1.0 μm) were strongly agglomerated. Such large agglomerates were

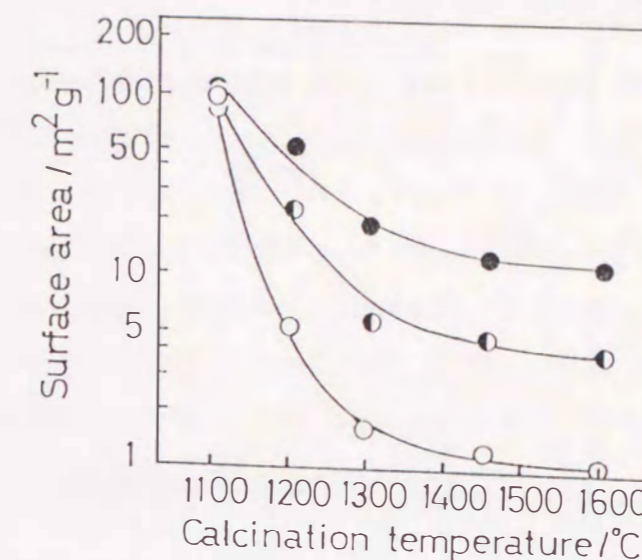Fig. 3.1. Temperature dependence of surface areas of $(BaO)_{0.14}$-$(Al_2O_3)_{0.86}$ and Al_2O_3.
● $(BaO)_{0.14}(Al_2O_3)_{0.86}$ (alkoxide)
◑ $(BaO)_{0.14}(Al_2O_3)_{0.86}$ ($BaCO_3$/γ-Al_2O_3)
○ Al_2O_3

a   b   c

1μm
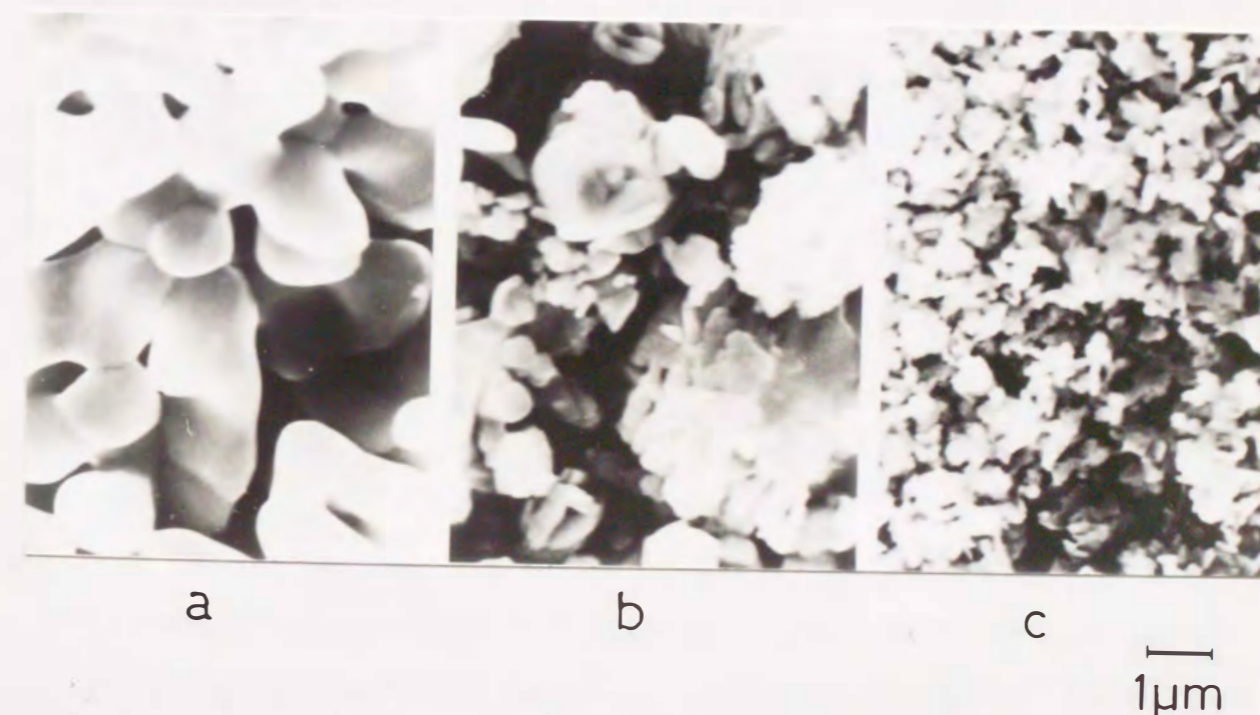
Fig. 3.2. SEM photographs of $BaAl_{12}O_{19}$ and Al_2O_3 after cal-cination at 1450 ℃. a) Al_2O_3, b) $BaAl_{12}O_{19}$ from $BaCO_3$/ γ-Al_2O_3, c) $BaAl_{12}O_{19}$ from alkoxides.
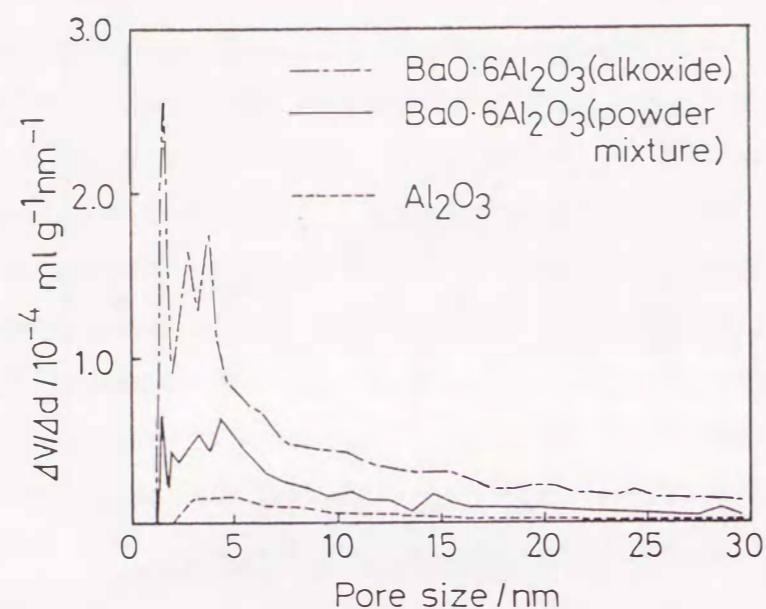
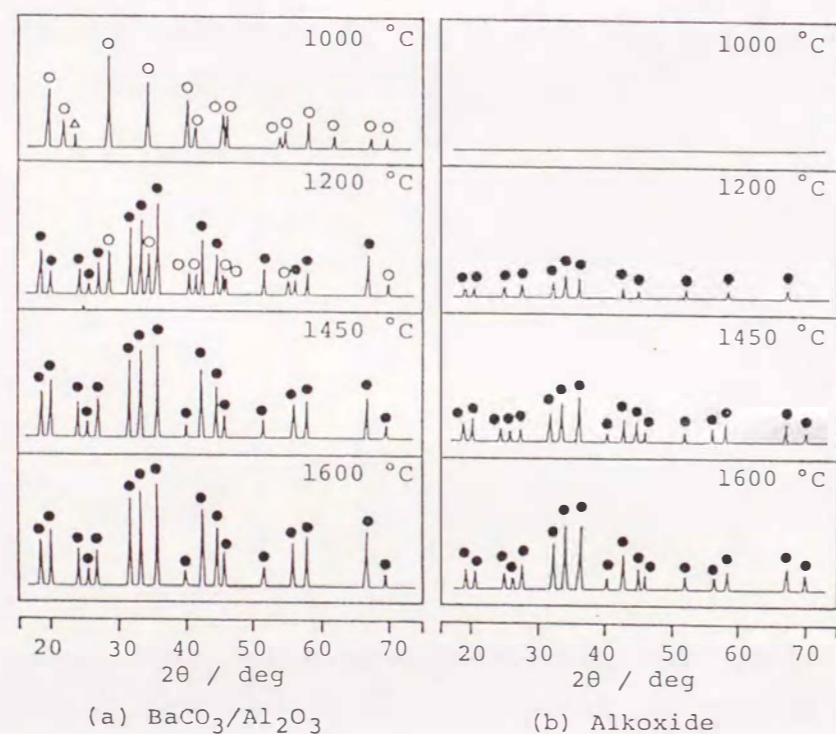Fig. 3.3. Pore size distributions of $BaAl_{12}O_{19}$ and Al_2O_3 after calcination at 1450 ℃.

Fig. 3.4. X-Ray diffraction patterns of $(BaO)_{0.14}(Al_2O_3)_{0.86}$ after calcination at various temperatures. a) Powder mixture of $BaCO_3$ and γ-Al_2O_3. b) Hydrolyzed alkoxides ● $BaAl_{12}O_{19}$,   ○ $BaAl_2O_4$,   △ $BaCO_3$

absent in the sample prepared from hydrolyzed alkoxides. The particles were in a granular shape with uniform (0.3 μm) size.

Pore size distributions of alumina and the $BaAl_{12}O_{19}$ samples were measured after calcination at 1450 ℃. The distribution was maximum at the pore size smaller than 10 nm (Fig. 3.3). The relative pore volume gradually decreased with increasing pore size. The barium hexaaluminate sample, in particular, that was prepared from alkoxides possessed obviously larger total pore volume than alumina. The sequence of total pore volume of three samples agreed with that of the surface area.

3.4 Analysis on Formation Process of Hexaaluminate
3.4.1 Powder X-Ray Diffraction Analysis

The phase diagram of the BaO-Al_2O_3 system indicates that the $BaAl_{12}O_{19}$ in the equilibrium state.[15] However, the $BaCO_3/$ γ-Al_2O_3 precursor underwent a complicated formation process to evolve this phase during the heating process as mentioned in Chapter 2. Figure 3.4 compares the X-ray diffraction patterns of $BaCO_3/\gamma$-Al_2O_3 mixtures and alkoxide-derived samples in a heating course. After calcination at 1000 ℃, the phase observed in $BaCO_3/\gamma$-Al_2O_3 sample was the equimolar compound ($BaAl_2O_4$) and a trace amount of $BaCO_3$, instead of the equilibrium phase ($BaAl_{12}O_{19}$). The sample at this calcination condition is almost completely composed of a mixture of $BaAl_2O_4$ and Al_2O_3, though the diffraction lines from the latter phase are too weak to be observed by due to its poor crystallinity. With a rise in calcination temperature, the diffraction lines from $BaAl_{12}O_{19}$ appeared and became intense. The formation of the equilibrium $BaAl_{12}O_{19}$ phase was completed after heating at 1450 ℃.

The samples from alkoxides, on the other hand, showed no

diffraction lines after heating at 1000 ℃. The diffraction lines only due to the $BaAl_{12}O_{19}$ phase appeared at 1200 ℃ (Fig. 3.4(b)). They became sharp and intense at elevated calcination temperatures, but the $BaAl_2O_4$ phase was not observed at any temperatures. X-ray diffraction data suggest the different formation process of $BaAl_{12}O_{19}$ from the two types of precursors. While powder mixtures of $BaCO_3/\gamma-Al_2O_3$ produced $BaAl_{12}O_{19}$ via formation of a metastable phase of $BaAl_2O_4$, hydrolyzed alkoxides produced $BaAl_{12}O_{19}$ directly at lower temperatures. Thus, the large surface area of alkoxide-derived $BaAl_{12}O_{19}$ appears to be closely related to the formation mechanism. However, X-ray diffraction gives only average information for bulk materials. An actual reason for the large surface area was investigated in detail from microscopic observation of particles under reaction in the following section.

3.4.2 Analytical Electron Microscope Analysis

$BaO-Al_2O_3$ samples submitted to AEM analysis are listed in Table 3.2.[16] XRD measurement after calcination at 1100 ℃ showed that only the equilibrium phase, $BaAl_{12}O_{19}$ was observed in the alkoxide-derived sample. The powder mixture sample consisted of $BaAl_2O_4$ as well as trace amounts of $BaCO_3$. After calcination at 1300 ℃, the diffraction pattern of the alkoxide-derived sample was basically unchanged. The powder mixture sample also contained $BaAl_{12}O_{19}$ at this temperature, but $BaAl_2O_4$ still remained. After calcination at 1100 ℃, the surface areas of both samples were similar (50 m^2/g), but they decreased sharply with calcination at 1300 ℃. The alkoxide-derived sample, however, retained a surface area (20.2 m^2/g) three times larger than the powder mixture sample (6.3 m^2/g).

Table 3.1 Surface areas and crystalline phases of $(BaO)_{0.14}$-$(Al_2O_3)_{0.86}$ for AEM analysis

Precursor	temperature / ℃	Surface area /m^2g^{-1}	Phase
$BaCO_3/\gamma-Al_2O_3$	1100	53.1	$BaAl_{12}O_{19}$ + Al_2O_3 + $BaCO_3$
	1300	6.3	$BaAl_{12}O_{19}$ + $BaAl_2O_4$
Hydrolyzed alkoxides	1100	47.5	$BaAl_{12}O_{19}$
	1300	20.2	$BaAl_{12}O_{19}$

(a) $BaCO_3/\gamma-Al_2O_3$ powder mixture

Figure 3.5 shows a TEM image (a), corresponding EDS spectra (b) and SAD patterns (c) for $BaCO_3/\gamma-Al_2O_3$ mixtures calcined at 1100 ℃. The sample consisted of fine particles (particle 1) and large columnar particles (particle 2) with the length of 200-500 nm. The EDS analysis and the SAD pattern with Debye-Scherrer rings showed that the fine particles are metastable alumina with poor crystallinity. On the other hand, only a Ba peak in the EDS spectrum was seen in the columnar particles and a single crystal SAD pattern indicated the lattice spacings of 0.64 and 0.53 nm in two orthogonal directions (Fig. 1c). These values agreed with the **b** and **c** unit cell dimensions of orthorhombic $BaCO_3$. The formation of $BaAl_2O_4$ was observed in the same sample both by X-

ray diffraction and by electron diffraction. However, the SAD patterns contain spots from unreacted Al_2O_3 and $BaCO_3$ phases.

After calcination at 1300 ℃, reaction products and their morphology changed as shown in Fig. 3.6. The agglomerates of fine alumina particles were no longer observed and considerable grain growth occurred. The EDS analyses indicated that the cation composition of particles 1 and 2 in Fig. 3.6a corresponds to $BaAl_{12}O_{19}$. A typical spectrum is shown in Fig. 3.6b. This is consistent with the SAD patterns of these particles, which could be indexed with respect to the [001] zone axis of $BaAl_{12}O_{19}$ (Fig. 3.6c). However, some non-equilibrium products were observed at this composition because of incomplete solid state reaction. Particle 3, which exhibits considerable grain growth, is pure alumina without including other cation components. This particle is thermally formed α-Al_2O_3 as can be judged from the SAD pattern (Fig. 3.6c). Particle 4 contains more Ba than the equilibrium composition. The Ba/Al atomic ratio, which is calculated from the integrated intensity ratio of $BaK\alpha/AlK\alpha$, was roughly six times as large as $BaAl_{12}O_{19}$, implying the composition of $BaAl_2O_4$. Thus, the composition of the product is still heterogeneous even after heating at 1300 ℃ due to incomplete solid state reaction between Al_2O_3 and $BaAl_2O_4$.

(b) Alkoxide-derived sample

As shown in Table 3.2, the surface area of $BaAl_{12}O_{19}$ is enhanced by the preparation from alkoxides. This process facilitates the direct formation of $BaAl_{12}O_{19}$ at low temperature, which is effective in retaining the large surface area during the heating process. Figure 3.7 shows the analysis result of alkoxide derived BaO-Al_2O_3 calcined at 1100 ℃. The sample, which predom-

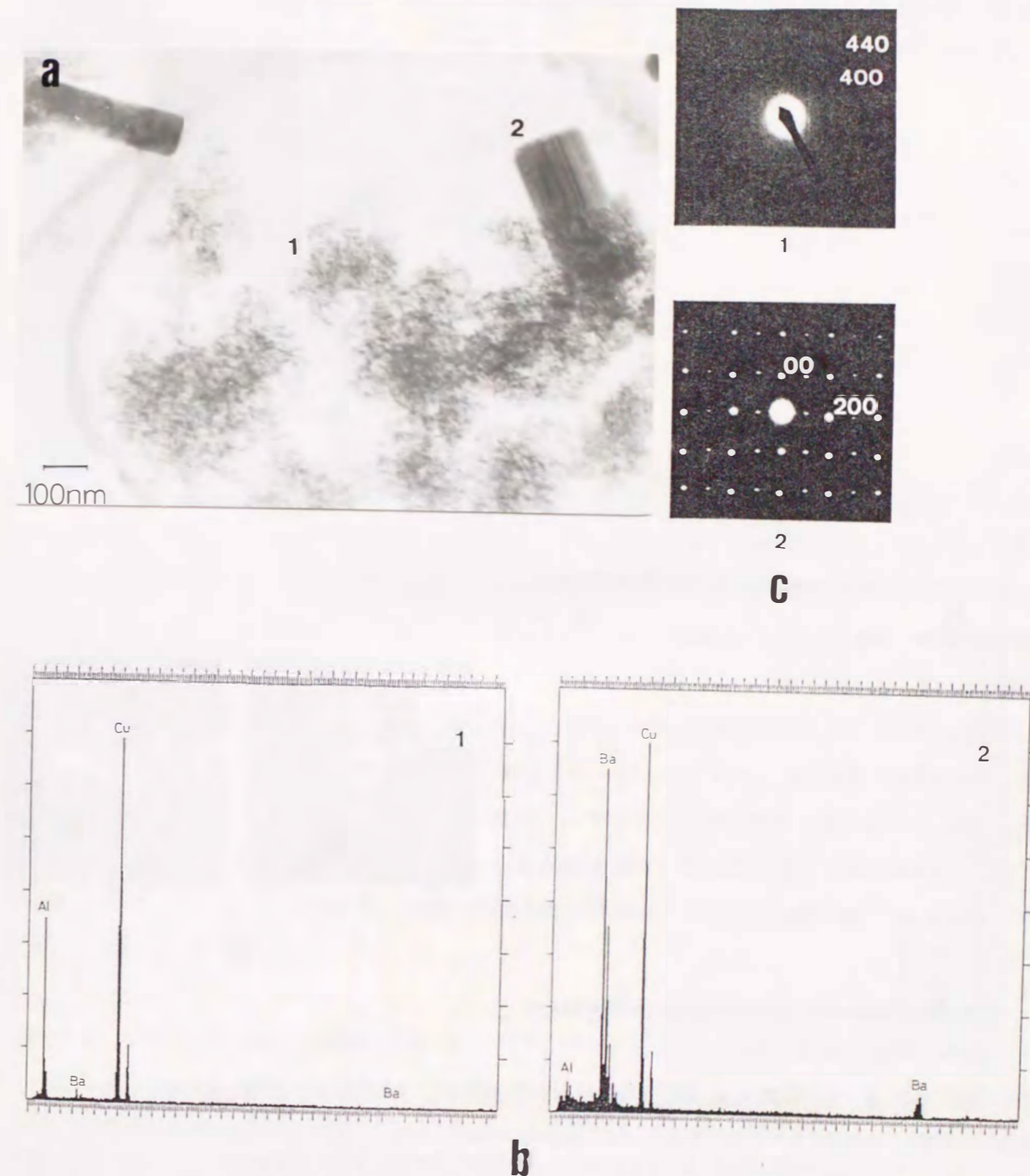Fig. 3.5. a)TEM photograph of $BaCO_3/\gamma$-Al_2O_3 powder mixtures calcined at 1100 ℃; b) and c) illustrate EDS results and SAD patterns taken from the numbered particles, respectively.
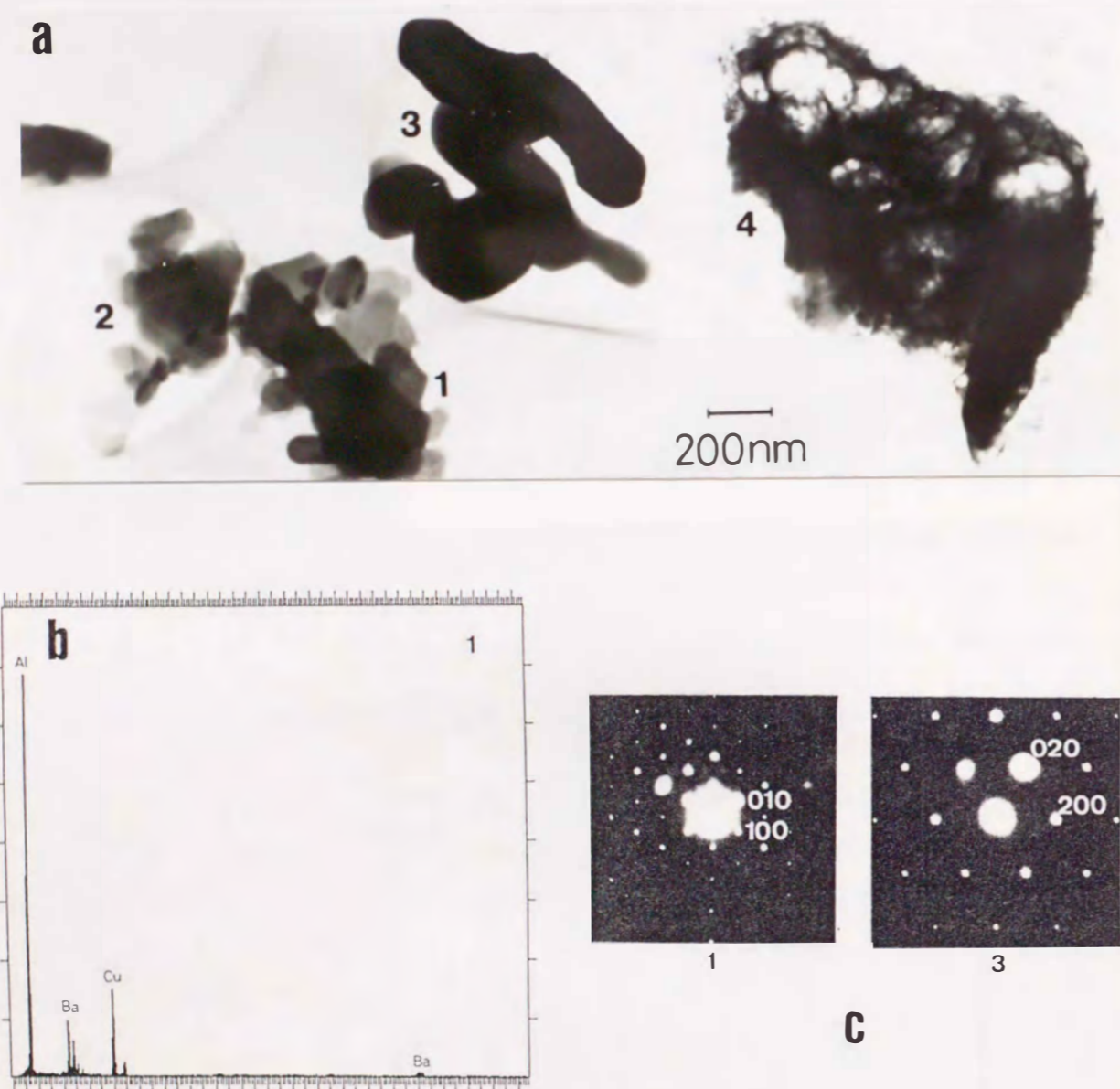
inantly consisted of the fine particles with a uniform size around 10 nm, exhibited Debye-Scherrer rings as shown in the SAD pattern. The d-spacings of the SAD rings match those of $BaAl_{12}O_{19}$. It is worth noting that these particles possess a composition close to that of $BaAl_{12}O_{19}$. Besides these fine particles, crystals of the same composition grew into planar particles (particle 2 in Fig. 3.7a) and the SAD patterns could be indexed with respect to the [001] zone axis of $BaAl_{12}O_{19}$ (Fig. 3.7b). Thus, the alkoxide-derived sample already produced the single phase of $BaAl_{12}O_{19}$ at 1100 ℃.

After calcination at 1300 ℃, it is apparent both from the shape of particles with facets and from the SAD patterns (Fig. 3.8a,b) that significant crystallization of $BaAl_{12}O_{19}$ occurred. Grain growth is accelerated by crystallization but the particle size was considerably small (ca. 100 nm) and uniform as compared to the powder mixture sample. In addition, it is clear from EDS analyses that all particles have the composition of $BaAl_{12}O_{19}$. Intermediate products and/or unreacted oxides, which existed in the calcined powder mixture sample, were scarcely observed in the alkoxide derived sample. It is apparent that the compositional homogeneity of alkoxide derived precursor is superior to that of the powder mixture.

3.4.3 Formation Mechanism and Microstructure of Hexaaluminate

XRD and AEM results indicate that the reaction process is different between the two precursors. In the powder mixture sample, some non-equilibrium phases still existed even at 1100-1300 ℃. In contrast, all particles showed uniform composition corresponding to $BaAl_{12}O_{19}$ in the alkoxide derived sample. Figure 3.9 shows electron micrographs of a typical particle

Fig. 3.6. a)TEM photograph of $BaCO_3/\gamma$-Al_2O_3 powder mixtures calcined at 1300 ℃; b) and c) illustrate EDS results and SAD patterns taken from the numbered particles, respectively. X-ray analyses of particles showed the following Ba/Al atomic ratios.

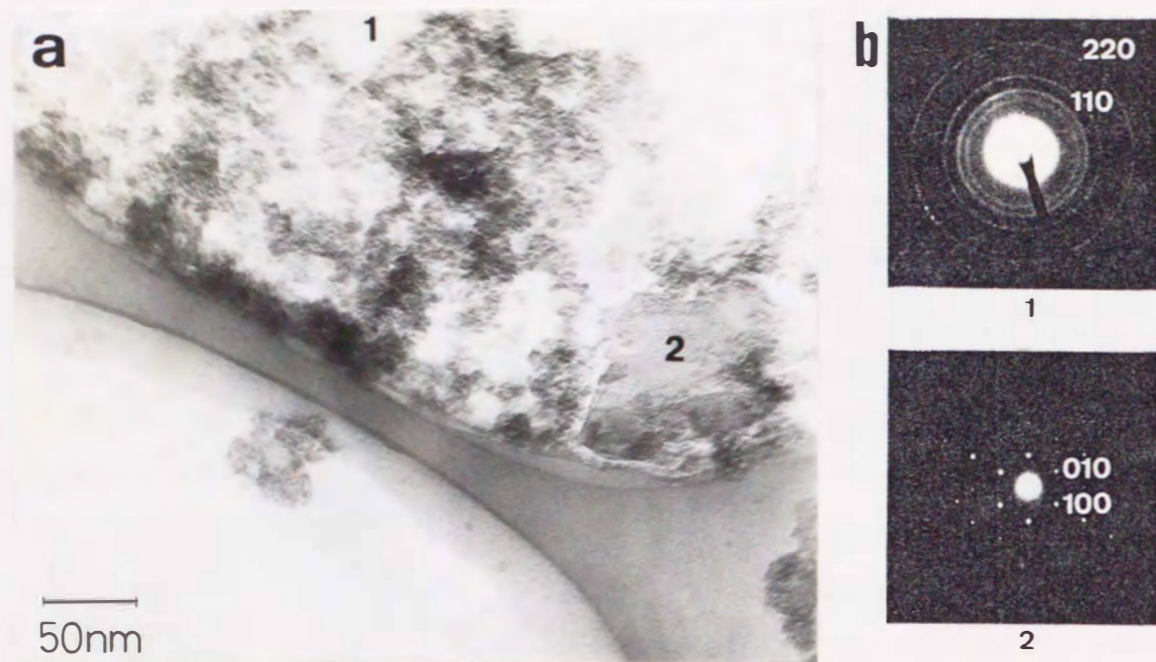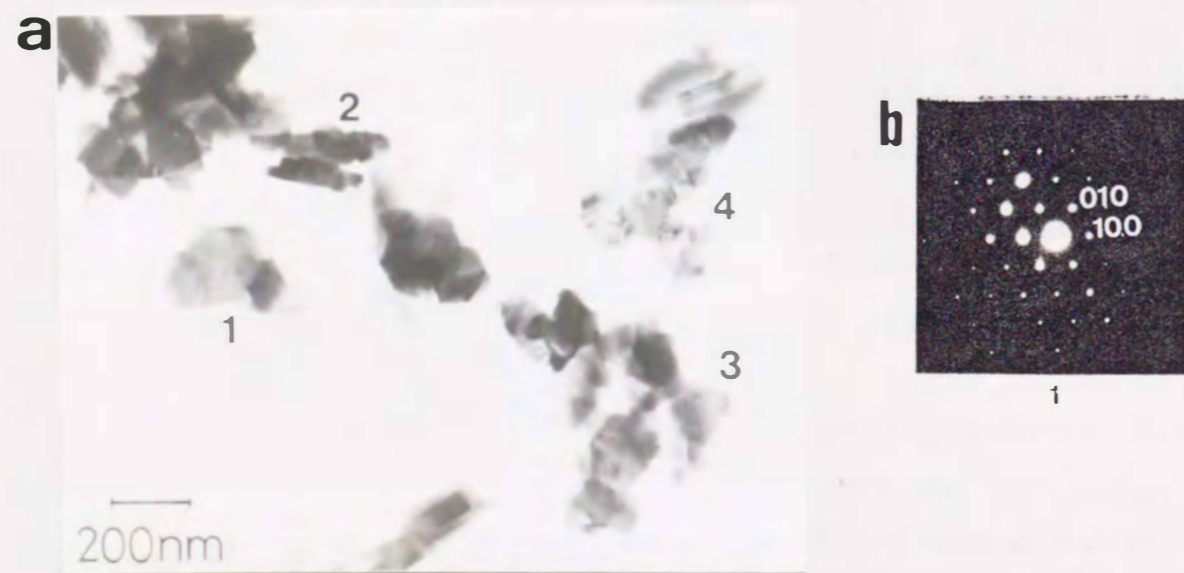| Particle No.	1	2	3	4
Ba/Al	0.086	0.105	0.000	0.430

Fig. 3.7. a)TEM photograph of the alkoxide derived $BaO-Al_2O_3$ calcined at 1100 °C; b) illustrates SAD patterns taken from the numbered particles.   X-ray analyses of particles   showed   the following Ba/Al atomic ratios.

Particle No.	1	2
Ba/Al	0.083	0.082

Fig. 3.8.   a)TEM photograph of the alkoxide   derived $BaO-Al_2O_3$ calcined at 1300 °C; b) illustrates SAD pattern taken from the numbered particles.   X-ray analyses of particles showed the following Ba/Al atomic ratios.

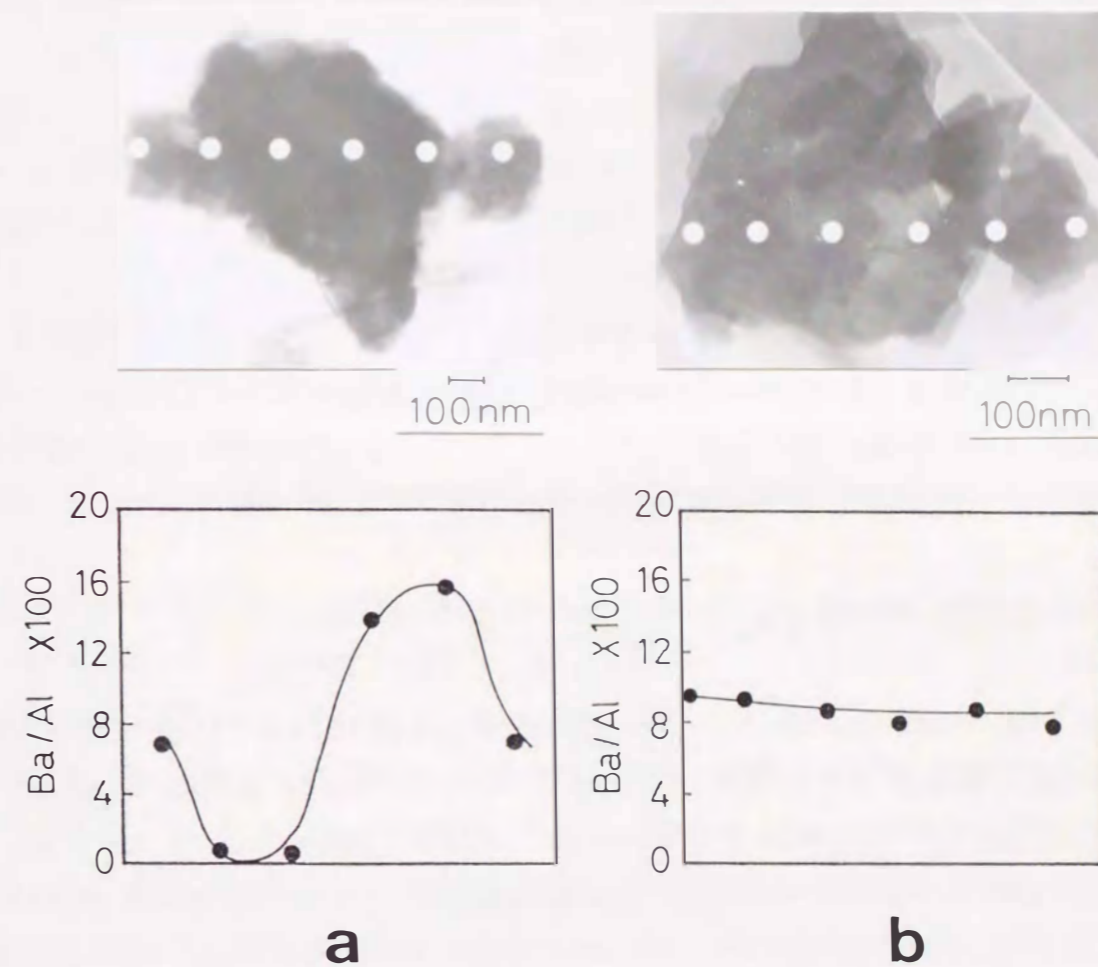| Particle No.	1	2	3	4
Ba/Al	0.086	0.077	0.081	0.084

Fig. 3.9.   TEM photographs and EDS Ba/Al atomic ratios of BaO-Al_2O_3 particles prepared from a) powder mixtures and b) hydrolyzed alkoxides. Diameter of an electron probe is 10 nm.

from the powder mixture (a) and that from the alkoxide derived sample (b) after calcination at 1300 °C. The ratios of Ba to Al were measured by EDS along the array of dots indicated in the figure. In every analysis, the diameter of an electron probe was about 10 nm. Ba/Al atomic ratios are plotted in the lower part of Fig. 3.9. The intraparticle composition is almost uniform for the alkoxide derived sample. In the powder mixture sample, however, the composition was heterogeneous due to the incomplete solid state reaction, which for this particle likely proceeded between $BaAl_2O_4$ and Al_2O_3 in this case (Fig. 3.9a).

From XRD and AEM results, the formation of $BaAl_{12}O_{19}$ from the two types of precursors appears to proceed as follows. In the powder mixtures, the formation of $BaAl_2O_4$ proceeds rapidly at the boundary of Al_2O_3 and $BaCO_3$ particles at low temperature(1100 °C).

$$BaCO_3 + Al_2O_3 \rightarrow BaAl_2O_4 + CO_2 \qquad (2)$$
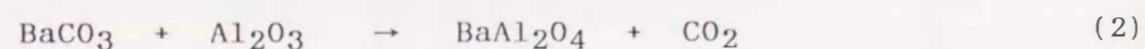
This reaction produces the large particles (500-1000 nm) of $BaAl_2O_4$ which do not contribute to the large surface area. The marked grain growth of alumina also takes place at the same temperature range. Barium hexaaluminate is subsequently produced in the second step by the reaction between the two kinds of particles.

$$BaAl_2O_4 + 5Al_2O_3 \rightarrow BaAl_{12}O_{19} \qquad (3)$$
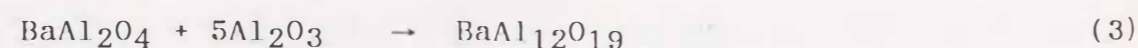
This step is very slow and requires higher temperatures when $BaAl_2O_4$ has grown into large particles. Similar formation steps are pointed out for other aluminates.[17,18] In $LaAl_{11}O_{18}$ formation for example[17], initially the reaction between La_2O_3 and Al_2O_3 produces $LaAlO_3$. It requires prolonged firing (> 100 h) to complete the diffusion-limited solid state reaction to produce $LaAl_{11}O_{18}$ from $LaAlO_3$ and Al_2O_3. Since the formation of $BaAl_{12}O_{19}$ starts at high temperatures(>1200 °C), the particles have already undergone some grain growth before the second solid-state reaction. As a result, the large surface area is not sufficiently available.

In the alkoxide derived sample, the formation of $BaAl_{12}O_{19}$ appears to exclude diffusion-controlled solid state reaction steps, since the components have already been mixed at a molecular level. The equilibrium phase crystallizes directly from the thermally decomposed hydrolyzed precursor.

$$(BaO)_{0.14}(Al_2O_3)_{0.86} \text{ (amorphous)} \rightarrow BaAl_{12}O_{19} \text{ (crystalline)} \qquad (4)$$

This is reflected in the absence of both intermediate products and considerable grain growth. In addition, hydrolyzed precursors consisted of very fine particles with a uniform size. This explains the large surface area and the uniform microstructure of the alkoxide-derived $BaAl_{12}O_{19}$. Once the single phase of $BaAl_{12}O_{19}$ has formed, surface area loss at elevated temperatures is suppressed successfully because the hexaaluminate structure shows the excellent resistance to grain growth and sintering.

3.5 Effect of Preparation Conditions on Surface Area of Alkoxide-Derived Hexaaluminate

3.5.1 Surface Area of Alkoxide-Derived Hexaaluminate

The surface area of alkoxide-derived powders is sensitive to some preparation conditions in the hydrolysis process such as the aging period of the hydrolyzed products and the amount of

water.[19,20] The amount of water added for hydrolysis is expressed as a molar ratio per metal isopropoxyl group ($R(H_2O/MOC_3H_7)$). The number of metal isopropoxyl groups, $-MOC_3H_7$, is the sum of $-AlOC_3H_7$ and $-BaOC_3H_7$. Figure 3.10 shows the effect of $R(H_2O/MOC_3H_7)$ on the surface area of $BaAl_{12}O_{19}$. The surface area was maximum (20.2 m^2/g) at $R(H_2O/MOC_3H_7)=0.5$, but decreased either by an increase or a decrease in the amount of water. The optimum condition, $R(H_2O/MOC_3H_7)=0.5$, agreed with the stoichiometric ratio for the hydrolysis of alkoxides. The effect of the amount of water is obvious when calcination was performed at lower temperature such as 1300 ℃. Figure 3.11 shows SEM photographs of precursors after a given amount of water was added to the alkoxide solution for hydrolysis. Corresponding to the two regions observed in the Fig. 3.12, the particle morphology was different between samples with $R(H_2O/MOC_3H_7)<0.5$ and $R(H_2O/MOC_3H_7)>0.5$. The hydrolyzed sample at $R(H_2O/MOC_3H_7)>0.5$ consisted of submicron particles, but the particle morphology and size were almost unchanged with increasing the amount of water as observed by SEM. In contrast, the particle size became larger when less water ($R(H_2O/MOC_3H_7)<0.5$) was used for hydrolysis. In this region, the amount of water is not enough for complete hydrolysis of the alkoxides. The microstructures of the hydrolysis products well reflect the surface area of the $BaAl_{12}O_{19}$. Large agglomerates and large precursor particles appear to result in a low surface area after calcination.

As shown in Fig. 3.12 the surface area increased with the initial aging period of hydrolyzed products and became almost constant after 12 h ($R(H_2O/MOC_3H_7)=10.0$). After 12 h of aging and subsequent calcination at 1300 ℃, the sample retained the surface area of 18.5 m^2/g, which is about double that of the

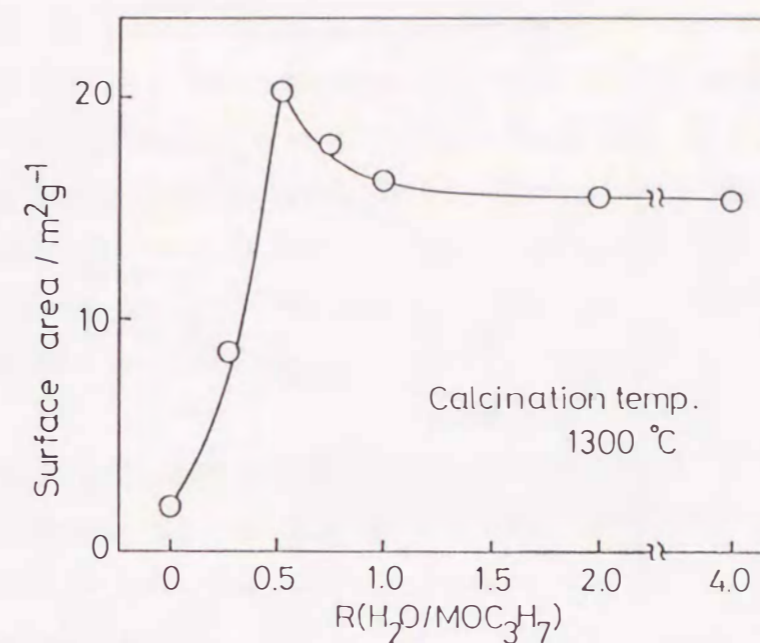Fig. 3.10. Effect of the amount of water added to alkoxides on the surface area of $BaAl_{12}O_{19}$. (12 h aging)
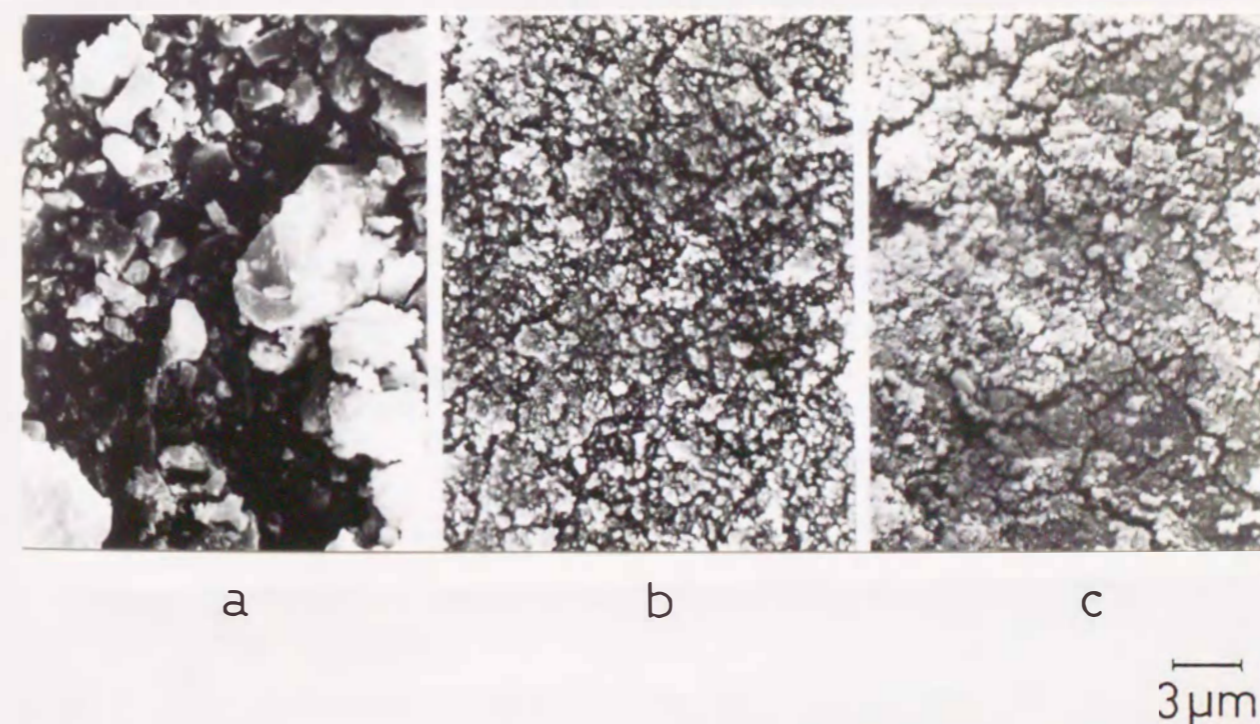

a   b   c

3 μm

Fig. 3.11. Microstructures of hydrolyzed precursors with various $R(H_2O/MOC_3H_7)$.
a) $R(H_2O/MOC_3H_7)=0.3$, b) 0.5, c) 1.0. (12 h aging)

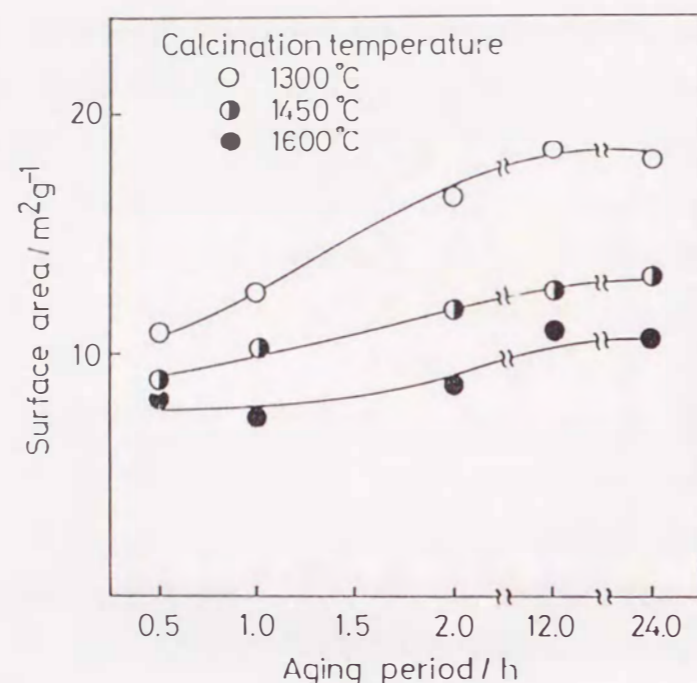Fig. 3.12. Effect of the aging period of hydrolyzed precursors
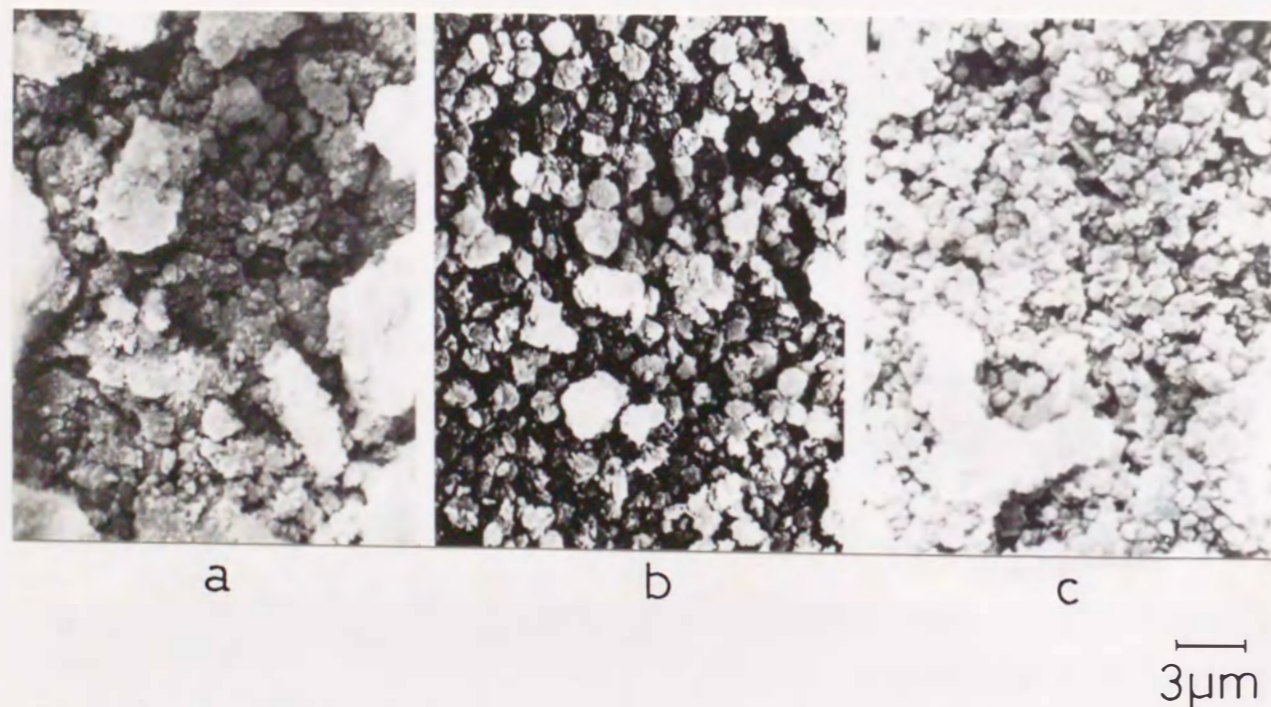on the surface area of $BaAl_{12}O_{19}$. $(R(H_2O/MOC_3H_7)=10.0)$

Fig. 3.13. Microstructures of hydrolyzed precursors with various
aging period.
a) 0.5 h, b) 2.0 h, c) 24.0 h $R(H_2O/MOC_3H_7=10.0)$

sample with 30 min of aging. The effect of the aging period was
investigated by microscopic observation of the hydrolysis pre-
cursors (Fig. 3.13). In the initial stage, the sample contained
large agglomerates (larger than 10 μm) which consisted of
submicron primary particles. With the aging progress, the size
of the agglomerate was reduced. After aging for 24 h, the sample
consisted almost entirely of equal sized particles and agglomer-
ates were rarely observed.

3.5.2 Thermal Behavior of Hydrolyzed Alkoxides

The decomposition of the hydrolyzed products $(R(H_2O/MOC_3H_7)=$
1.0, 12 h aging) was analyzed by in situ IR measurements. The IR
spectra obtained after heating in vacuo at various temperatures
are shown in Fig. 3.14. At room temperature, the hydrolyzed
product showed the absorption band of the H-O-H bending vibration
around 1640 cm^{-1}. This band, being attributed to the physisorbed
water, completely disappeared after evacuation at 200 ℃. The
bands at 3000-3500 cm^{-1} probably correspond to the O-H stretching
mode of the metal hydroxides in the hydrolyzed precursors. These
peaks were weakened at elevated temperatures due to the thermal
decomposition of metal hydroxides to mixed oxides. The O-H bands
disappeared at 400 ℃ after complete decomposition.

Figure 3.15 shows the DTA/TG curves of hydrolyzed precur-
sors prepared under various $R(H_2O/MOC_3H_7)$ conditions. A broad
endothermic peak below 100 ℃, which was observed in every alkox-
ide-derived sample, is attributed to the elimination of physi-
sorbed water. A large and sharp endothermic peak with a 25%
weight loss appeared in the sample with $R(H_2O/MOC_3H_7)=10$ around
250 ℃. From the IR result, this weight loss can be attributed to
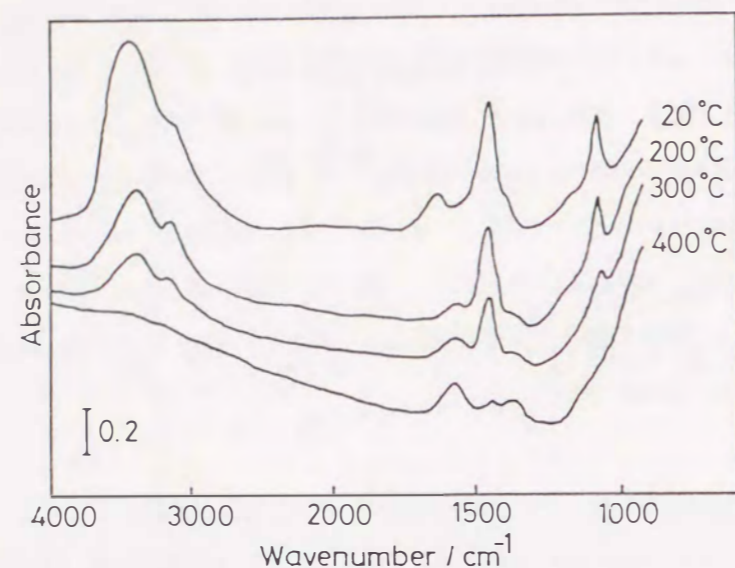dehydration accompanied by the thermal decomposition of metal

Fig. 3.14. Change of infrared spectrum of hydrolyzed alkoxides during the course of heating. Preparation condition of samples : $R(H_2O/MOC_3H_7)=1.0$, 12 h aging
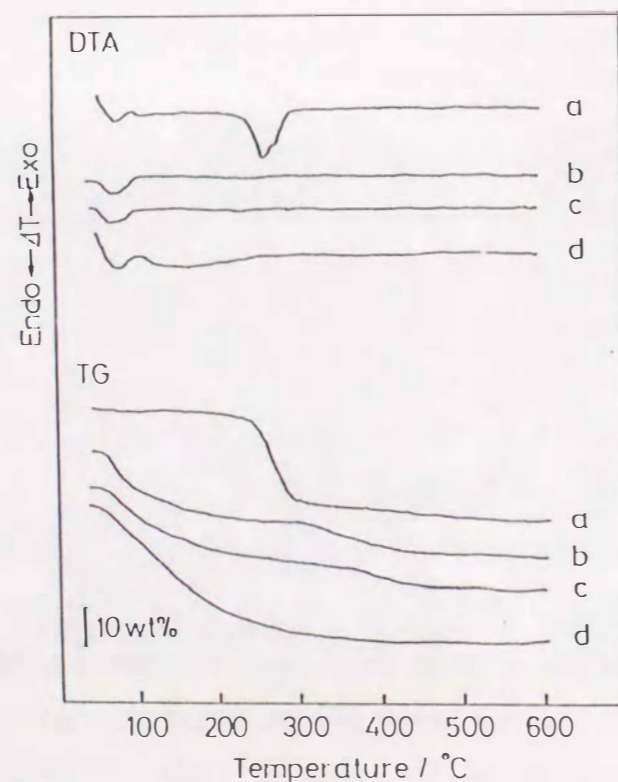

Fig. 3.15. DTA/TG analyses of the hydrolyzed precursors prepared under various $R(H_2O/MOC_3H_7)$ conditions.
a) $R(H_2O/MOC_3H_7)=10.0$, b) 2.0, c) 1.0, d) 0.5.

hydroxides. While the similar behavior was observed in the samples with $R(H_2O/MOC_3H_7)<2.0$ at 250-400 ℃, their small weight loss corresponds to the small content of metal hydroxides in the hydrolyzed product.

3.5.3 Effect of Preparation Condition in Alkoxide Process

As described above, surface area of alkoxide-derived sample was affected by the amount of water and by the aging period after hydrolysis. The change in surface area with the amount of water is apparently divided into two regions as shown in Fig. 3.10.[2,3,5] The stoichiometric amount of water for the decomposition of alkoxides is $R(H_2O/MOC_3H_7)=0.5$.

$$2 \ -M-(OC_3H_7) \ + \ H_2O \ \rightarrow \ -M-O-M- \ + \ 2 \ C_3H_7OH \qquad (5)$$
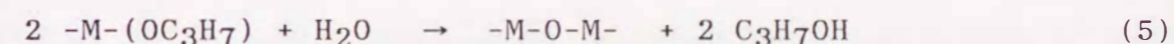
At $R(H_2O/MOC_3H_7)<0.5$, some fraction of the oxide is produced by hydrolysis (reaction(5)) but other fraction is produced by pyrolysis of the residual metal alkoxides. The increase in surface area in this region indicates that pyrolysis of the alkoxides does not contribute to the large surface area. Namely, a substantial amount of hydrolysis is required to produce a large surface area. The particle size of the incompletely hydrolyzed product is two orders of magnitude larger than that of the sample at $R(H_2O/MOC_3H_7)>0.5$ (Fig. 3.11).

At the second region ($R(H_2O/MOC_3H_7)>0.5$), the surface area decreases with an increase in $R(H_2O/MOC_3H_7)$ (Fig. 3.10). The partial formation of hydroxides (reaction(6)) is included due to the presence of excessive water in this region.[2,3,5]

$$M(OC_3H_7)_n \ + \ n \ H_2O \ \rightarrow \ M(OH)_n \ + \ n \ C_3H_7OH \qquad (6)$$
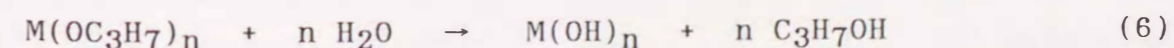
As the amount of water increases, the reaction (6) becomes dominant, resulting in a high content of hydroxide groups in the product. The hydroxides thus formed are thermally decomposed into oxides accompanying elimination of water in the temperature range 250-400 °C as was observed by TG (Fig. 3.15). The weight loss in this temperature range increased with $R(H_2O/MOC_3H_7)$, corresponding to the increase in the hydroxide content in the precursors. The formation temperature of $BaAl_{12}O_{19}$ from the sample with a low extent of hydrolysis $(R(H_2O/MOC_3H_7)<1.0)$ was near 1100 °C, while it is above 1200 °C for the sample with large $R(H_2O/MOC_3H_7)$. These results indicate that the precursors with homogeneous composition can be obtained near the stoichiometric hydrolysis condition. Actually, it is well known that hydrolysis of alkoxides in the presence of an excess water sometimes leads to dissolution-precipitation of resultant hydroxides.[6] In the binary system such as Ba-Al, this may result in decrease of homogeneity of precursors.

The effect of the aging period in Fig. 3.12 is smaller than that of the amount of water. Since the thermal decomposition of hydrolyzed alkoxides was scarcely influenced by the aging period as revealed by IR and TG/DTA, the chemical structure of products is not influenced by the aging period. However, the increase in surface area with aging appears to be related to the extent of agglomeration of hydrolyzed products (Fig. 3.13). The aging of hydrolyzed products in the presence of excessive water likely reduced the agglomeration of particles and brought about a high dispersion state. Large agglomerates, which are observed at a short aging period, grow into large particles in the course of heating. This only leads to the decrease in the surface area of $BaAl_{12}O_{19}$.

3.6   Conclusion

Preparation by hydrolysis of metal alkoxides is a superior process in deriving the large surface area hexaaluminate. The surface area of 11 m^2/g after calcination at 1600 °C could not be attained by conventional support oxides so far. The relation between microstructures and the formation process of $BaAl_{12}O_{19}$ in two precursors, i.e., powder mixtures and hydrolyzed alkoxides, was investigated by using XRD and AEM. When prepared from a powder mixture of $BaCO_3/\gamma-Al_2O_3$, $BaAl_{12}O_{19}$ was produced via formation of a metastable phase of $BaAl_2O_4$ upon heating. Since this route requires a slow diffusion-limited step at high temperatures and the $BaAl_2O_4$ is easily sintered, the product underwent considerable grain growth. On the contrary, since an alkoxide-derived precursor consists of a homogeneous mixture of the components, the equilibrium phase directly crystallized from the amorphous precursor at 1100 °C. This is extremely effective in producing the fine particle of $BaAl_{12}O_{19}$ with high thermal stability.

In the alkoxide process, the amount of water added for hydrolysis and the aging period of hydrolyzed precursors influenced the surface area of alkoxide-derived hexaaluminate. These effects of preparation conditions originated from the difference in microstructure and the chemical structure of hydrolyzed precursors. Monodispersed fine precursor particles with high chemical homogeneity are necessary for the large surface area hexaaluminate.